TDA Progress Report 42-119

November 15, 1994

Radio–Planetary Frame Tie From Phobos-2 VLBI Data

C. E. Hildebrand, B. A. Iijima, P. M. Kroger, and W. M. Folkner
Tracking Systems and Applications Section

C. D. Edwards
DSN Technology and Science Office

In an ongoing effort to improve the knowledge of the relative orientation (the "frame tie") of the planetary ephemeris reference frame used in deep space navigation and a second reference frame that is defined by the coordinates of a set of extragalactic radio sources, VLBI observations of the Soviet Phobos-2 spacecraft and nearby (in angle) radio sources were obtained at two epochs in 1989, shortly after the spacecraft entered orbit about Mars. The frame tie is an important systematic error source affecting both interplanetary navigation and the process of improving the theory of the Earth's orientation. The data from a single Phobos-2 VLBI session measure one component of the direction vector from Earth to Mars in the frame of the extragalactic radio sources (the "radio frame"). The radio frame has been shown to be stable and internally consistent with an accuracy of 5 nrad. The planetary ephemeris reference frame has an internal consistency of approximately 15 nrad. The planetary and radio source reference frames were aligned prior to 1989 with an accuracy of approximately 250 nrad, using Earth-based optical data and measurements of occultations of the radio source 3C273 by the Moon. The Phobos-2 VLBI measurements provide improvement in the accuracy of two of the three angles describing a general rotation between the planetary and radio reference frames. A complete set of measurements is not available because data acquisition was terminated prematurely by loss of the spacecraft. The analysis of the two Phobos-2 VLBI data sets indicates that, in the directions of the two rotation components determined by these data, the JPL planetary ephemeris DE200 is aligned with the radio frame as adopted by the International Earth Rotation Service within an accuracy of 20–40 nrad, depending on direction. The limiting errors in the solutions for these offsets are spacecraft trajectory (20 nrad), instrumental biases (19 nrad), and dependence of quasar coordinates on observing frequency (24 nrad).

I. Introduction

Planetary approach navigation is crucial to the success of many interplanetary missions. Whether it be for targeting a planetary flyby to carry out a gravity assist trajectory or for planning a maneuver to enter into a closed orbit about a target planet, the planetary approach phase almost always imposes key navigation requirements. Minimizing target-relative trajectory errors results in fuel savings that can

extend mission lifetimes and enhance the total scientific return. Future missions may employ aerobraking and aerocapture maneuvers to provide more efficient orbit insertion. These techniques can impose stringent constraints on navigation accuracy, as the spacecraft trajectory must pass through a narrow atmospheric entry corridor.

Earth-based tracking of radio signals from interplanetary spacecraft provides essential information for navigating deep space missions to their targets. The radio metric data types acquired by stations on the Earth include range from the station to the spacecraft, range rate via the Doppler shift of the spacecraft signal frequency received at the station, and interferometric delay and delay rate, in which very long baseline interferometry (VLBI) is used to obtain the angular position and velocity of the spacecraft in a reference frame of quasars (the "radio frame"). For many missions (e.g., Magellan, Ulysses), Earth-based radio metric observations are the only data available for orbit determination.

Spacecraft-based optical observations of a target body against the stellar background can provide information on the spacecraft-target relative position in the two directions orthogonal to the spacecraft-target line of sight. Since the position accuracy scales directly with distance from the target body, spacecraft imaging data are useful only during the latter stages of planetary approach. Also, the line-of-sight component of relative position is typically not well determined by onboard optical data. Thus, even for spacecraft equipped with onboard imaging systems, Earth-based radio data play an important role in determining the full spacecraft target–relative state vector.

The concept of a reference frame is central to navigation. An inertial reference frame is assumed in modeling the spacecraft trajectory and in the analysis of spacecraft position measurements. There are two main reference frames involved in the interplanetary navigation process. One frame is defined by the positions of distant radio sources; the other is defined in constructing the planetary ephemeris. The ephemeris gives the positions of the gravitational bodies affecting the spacecraft trajectory as well as the location of the target body. The radio reference frame is important in the reduction of spacecraft position measurements because the rotational orientation of the Earth, which has random components, is monitored and reported routinely in the radio reference frame. Thus, the inertial locations of Earth tracking stations are implicitly referred to the radio frame. With range and Doppler observables, the radio frame position of a spacecraft during interplanetary cruise can be determined with an accuracy of about 100–200 nrad. More precise spacecraft positions (5–10 nrad) can be obtained with differential spacecraft–quasar VLBI observations that directly measure the angular position of the spacecraft relative to selected quasars.[1,2,3] To most effectively exploit the accuracy of spacecraft interplanetary cruise trajectories given by Earth-based radio metric tracking, it is necessary that the target body position also be accurately determined in the radio frame.

The orientation offset between the planetary and radio reference frames, which may be parameterized as three small rotation angles collectively referred to as the "frame tie," was known to an accuracy of 100–200 nrad at the time the observations described herein were planned. This uncertainty greatly exceeds the accuracy attainable with Earth-based radio tracking techniques and is a limiting error for planetary approach navigation. As a result, several efforts have been initiated in recent years to improve the tie between the planetary and radio frames. Observations of the millisecond pulsar PSR 1937+21 [1] and comparisons of VLBI and lunar laser ranging (LLR) observations [2] have provided tentative

[1] J. S. Border, "Analysis of ΔDOR and ΔDOD Measurement Errors for Mars Observer Using the DSN Narrow Channel Bandwidth VLBI System," JPL Interoffice Memorandum 335.1-90-026 (internal document), Jet Propulsion Laboratory, Pasadena, California, May 15, 1990.

[2] W. M. Folkner, P. M. Kroger, and C. Hildebrand, "Preliminary Results From VLBI Measurement of Venus on September 12, 1990," JPL Interoffice Memorandum 335.1-92-25 (internal document), Jet Propulsion Laboratory, Pasadena, California, October 1992.

[3] W. M. Folkner, P. M. Kroger, and B. A. Iijima, "Results From VLBI Measurement of Venus on March 29, 1992," JPL Interoffice Memorandum 335.1-93-22 (internal document), Jet Propulsion Laboratory, Pasadena, California, July 1993.

measurements of the frame tie to an accuracy of 25–50 nrad. Several other, earlier determinations are discussed in [3].

Differential VLBI observations of a spacecraft in orbit about a planet provide a direct means of measuring the frame tie, as depicted in Fig. 1. Conventional Doppler tracking of a planetary orbiter typically can provide planet-relative spacecraft positions with kilometer- or sub-kilometer-level accuracy. With VLBI time delay measurements, differenced between the spacecraft and angularly nearby quasars to cancel common measurement errors, the spacecraft angular position (and thus the planet angular position as well) can be precisely determined in the quasar reference frame. The positions of the remaining bodies of the solar system are then also tied to the quasar frame to the accuracy of the relative angular position errors of the ephemerides. Newhall et al. [4] and Niell et al. [3] used a similar technique to estimate corrections to Mars' and Venus' right ascensions and declinations with data from the Viking and Pioneer Venus orbiters. These data were not VLBI time delays, but rather phase delay rates. Differential delay measurements from the Soviet Venus–Halley (VEGA) spacecraft as they flew past Venus were analyzed in [5].

In 1988, the Soviet Union launched two spacecraft, Phobos-1 and -2, to explore Mars and its moon Phobos. One of the scientific goals of the mission was a 5-nrad frame tie using VLBI measurements from a lander on the moon's surface.[4] Although both spacecraft were lost before completing their missions, Doppler and VLBI tracking data acquired from Phobos-2 in orbit about Mars have provided for an improved frame-tie determination. This article describes the analysis of the Phobos Mission (PHOBOS) frame-tie VLBI data and presents the resulting estimates of two components of the rotational offset between the frame of JPL planetary ephemeris DE200 [6,7] and the radio frame adopted and maintained by the International Earth Rotation Service (IERS) [8].

The following section contains a more detailed description of the radio and planetary reference frames within which the data presented here were analyzed. The PHOBOS VLBI observations are summarized in Section III. Section IV contains the analysis of measurement information content and error sources. The strategy for estimating the frame-tie parameters is given in Section V, and a reference solution is obtained. Consistency of solutions with variations of data set and fitting strategy is also examined. The PHOBOS result is compared with a frame tie derived from lunar laser ranging data and VLBI observations of natural sources. Section VI gives a brief discussion of further opportunities to improve the frame tie.

II. Reference Frames

A. IERS Reference Frames and Earth Orientation Parameters

The radio reference frame is based on the observed positions of extragalactic radio sources. The source positions are measured using VLBI, as shown in Fig. 2. Two widely separated radio antennas record the signal from the radio source. The recorded signals are processed to find the time delay, τ, which is the difference in arrival times at two stations. The time delay is approximately given by

$$\tau = \frac{1}{c}\left(\vec{B}\cdot\hat{S}\right)$$

where $\vec{B}$ is the vector pointing from (the inertial location of) station 1 to station 2 and $\hat{S}$ is a unit vector in the direction of the source. The observation of a single source thus gives the angle between the baseline vector and the direction to the source. By observing a number of sources widely scattered over the sky, the relative positions of the sources can be inferred along with the length and direction of the baseline vector.

[4] R. A. Preston, personal communication, Tracking Systems and Applications Section, Jet Propulsion Laboratory, Pasadena, California, 1991.

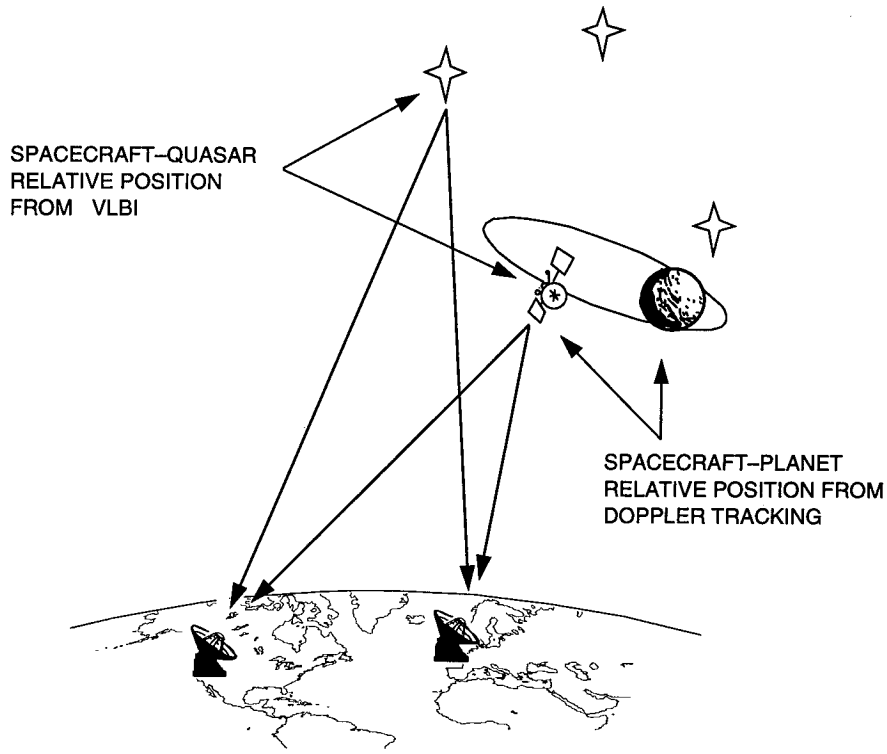

Fig. 1. Spacecraft–quasar differential VLBI geometry.

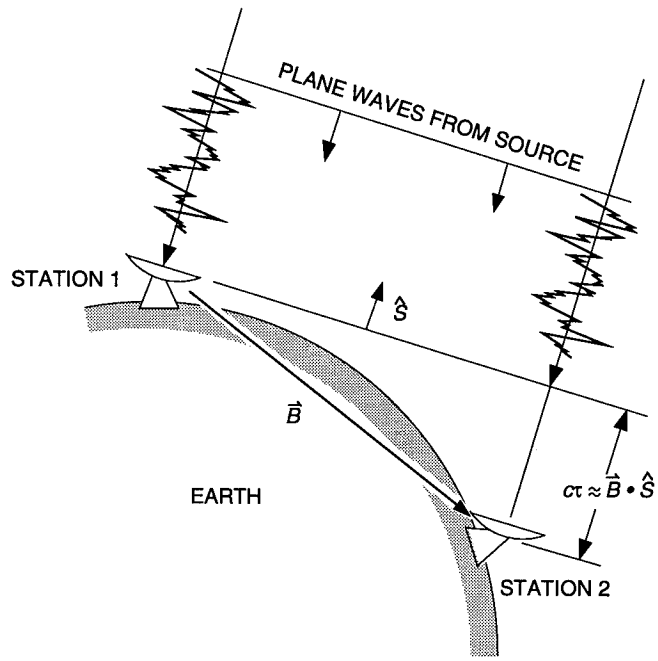

Fig. 2. VLBI geometry.

Since angles are measured only between the baseline vector and radio source directions, there is some arbitrariness in the definition of the direction of the coordinate axes. The celestial axes are traditionally defined in terms of the normal to the Earth's equator and the intersection of the equator and the ecliptic at some reference epoch (such as J2000). Because the Earth's rotation changes the baseline orientation with a diurnal signature, the VLBI data are sensitive to the equator of date. But these VLBI data are not sensitive to the position of the ecliptic. Before 1984, the orientation of the radio frame catalog about the equatorial pole was set by assigning a value to the right ascension of the source 3C273B based on observations of the occultation of this source by the Moon [9]. This choice of reference frame definition was found to be inadequate at the 5-nrad level of accuracy typical of modern VLBI measurements for two reasons: (1) The extrapolation of the equator of date to the equator of the reference epoch proved to be problematical, in that the standard theory for the motion of the equatorial pole is not accurate at the 5-nrad level, and (2) the source 3C273B has an apparent radio position that changes with time due to variations in source structure.

To avoid problems with changes in radio frame definition caused by variations in the model for motion of the Earth's pole and in the defined right ascension, the IERS in 1984 established a celestial reference frame by adopting coordinates for more than 20 commonly observed quasars with relative positions consistent at the 5-nrad level [10]. This celestial reference frame has been stable to better than 5 nrad since 1984 and is in approximate agreement with the Earth's equator and equinox of J2000 [8].

Given this definition of the celestial frame, it is necessary to define the zero point of baseline orientation. The IERS has specified positions (in terms of overall orientation) of a network of Earth tracking stations that define an "Earth-fixed" or terrestrial frame. This network includes VLBI antennas as well as sites for other techniques that can measure Earth orientation, including satellite laser ranging, lunar laser ranging, and Global Positioning System sites [11]. The network positions are continually updated as relative position information is improved. However, the overall orientation of the network is fixed so that the orientation of the Earth can be routinely monitored and reported in terms of the angles between the defined terrestrial network and the defined celestial frame.

B. Planetary Ephemeris Reference Frames

Range observations to planetary orbiters and landers, and radar ranges to the planetary surfaces, have provided a wealth of data on the motions of the planets in the solar system. Relative positions of Earth and Mars during the Viking lander ranging data arc (1976–1982) were known to an accuracy of a few nanoradians. Since then, the errors in relative longitudes have increased with time at a rate on the order of 1 nrad/yr [12]. The positions of Mercury and Venus relative to Earth have been determined to an accuracy of tens of nanoradians from planetary ranging data. Outer planets are known to lesser accuracy, based on spacecraft radio metric data during encounters, optical observations, and limited interferometric observations. For example, Jupiter's position is currently known to an accuracy of about 200 km, or 250 nrad, relative to Earth's orbit.

Beginning with JPL ephemeris DE200, the origin of right ascension for the planetary frame has been the dynamical equinox as determined from lunar laser ranging (LLR) data. LLR data are sensitive to the Earth's equator through the diurnal signature due to Earth rotation, and to the ecliptic through the effect of the luni-solar precession on the Earth–Moon distance. The LLR data determine the dynamical equinox at a mean data epoch of 1980 with an accuracy of approximately 5 nrad [12]. The ecliptic longitude of the Earth is determined to 15 nrad. The distributed ephemerides, however, are referred to the epoch J2000 rather than 1980. The uncertainty in predicting the difference in the equator of J2000 and the equator of 1980 is approximately 50 nrad. In general, each successive distributed ephemeris uses a longer arc of LLR data, which changes the estimate of the equator of J2000, so that the reference frames of two ephemerides are slightly different.

The distributed ephemerides do not contain information on the model for the motion of the Earth's pole that was used in defining the frame. Thus, angular offsets between different ephemerides cannot be

ascertained by comparing the orientations of the equator and equinox of date, but only by examining the tabulated positions of the planets. The relative positions of Earth and Mars are known to approximately 15 nrad, which is at least a factor of five better than the relative position accuracy of any other pair of bodies from the planetary ephemerides. Consequently, frame-tie comparisons between ephemerides, or between an ephemeris and the radio frame, have the most consistency and accuracy when based on the relative orientation of the orbit of the Earth and/or Mars in the two frames.

III. Data Acquisition

A. Observation Summary

The PHOBOS frame-tie data consist of two passes of VLBI observations of the Phobos-2 spacecraft and angularly nearby quasars. The PHOBOS data were recorded with the DSN wide-channel bandwidth (WCB) VLBI system, which is the DSN realization of the Mark III system developed for radio astronomy applications. Angular accuracy in the range of 1–5 nrad has been achieved with WCB observations of quasars [13,14]. The PHOBOS frame-tie data are the first interplanetary spacecraft–quasar differential VLBI measurements obtained with the WCB system.

The observing time in both passes was 1 hr. During the first pass on February 17, 1989, data were acquired by the DSN stations at Goldstone and Madrid and by the 76-m Lovell telescope at Jodrell Bank in England. Although the addition of Lovell improved the baseline geometry somewhat, the main reason for its inclusion was to enhance reliability. The second pass occurred on March 25, 1989, on the Goldstone–Canberra baseline. The DSN 70-m antennas were used for both passes, as they were the only DSN stations equipped to receive at the Phobos-2 spacecraft transmit frequency of approximately 1.7 GHz.

The Phobos-2 spacecraft and three extragalactic radio sources (see Fig. 3 for source geometry) were observed sequentially, not simultaneously, during each pass, according to the schedule in Fig. 4. Since uncalibrated path delay changes due to variations in solar plasma, troposphere, or ionosphere between spacecraft and radio source observations can degrade the accuracy of the measured differential delay, the observation sequences provided for sampling the temporal variation of measurement errors via multiple observations of a given source. Similarly, observations of quasars at various separation angles from the spacecraft were included to yield some indication of the spatial variation of media delays. An additional factor affecting the PHOBOS observation sequences was that the quasars with the smallest angular separations from Mars were relatively weak. Observations of well-known sources with high correlated flux density were included to provide a margin of reliability in case these weak sources could not be detected.

B. PHOBOS Frame-Tie Radio Sources

Of the six sources selected for the PHOBOS frame-tie experiments, the position of only one (0235+164) was known to an accuracy of 10 nrad or less. The positions of the remaining sources were determined with data from four DSN WCB VLBI passes in July and September of 1989—three passes on the Goldstone–Madrid baseline and one on the Goldstone–Canberra baseline. All data were acquired at 34-m stations.

During the astrometric passes, the PHOBOS sources and several quasars whose positions were precisely known were observed repeatedly over periods of about 8 hr. Data were acquired at both S-band (2.3 GHz) and X-band (8.4 GHz) so that signal delays due to charged particles of the ionosphere and the solar plasma could be calibrated. These observations were then combined with other DSN VLBI astrometric data. The entire data set was processed through the VLBI parameter estimation program, MODEST [15], to provide a quasar catalog, as well as Earth orientation parameters for each VLBI pass [16]. These results were then incorporated into the radio source catalog RSC(IERS) 91 C 01 of the International Earth Rotation Service. The 1-σ rss error in the estimated angular positions of the PHOBOS sources is about $15\sqrt{2}$ nrad (see Table 1 and the discussion in Section IV.B).

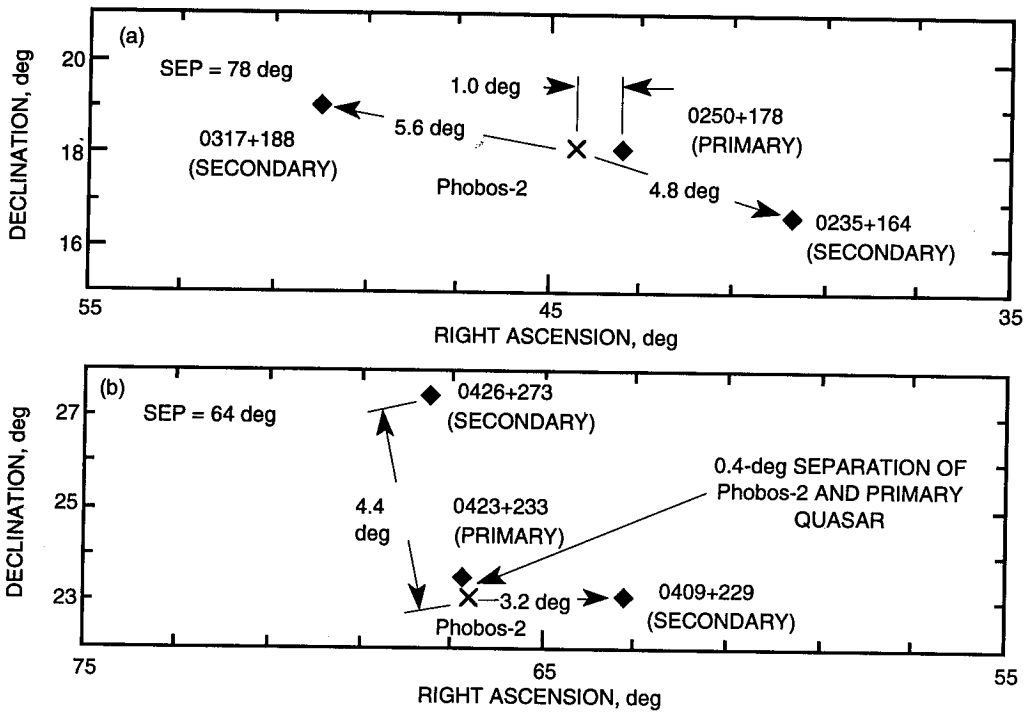

Fig. 3. Angular separation of the Phobos-2 spacecraft (X) from the radio sources (◆): (a) February 17, 1989, and (b) March 25, 1989. The source with the smallest angular offset from the spacecraft on each day is denoted as the primary source. SEP is the angular separation of the spacecraft and the Sun as viewed from Earth.

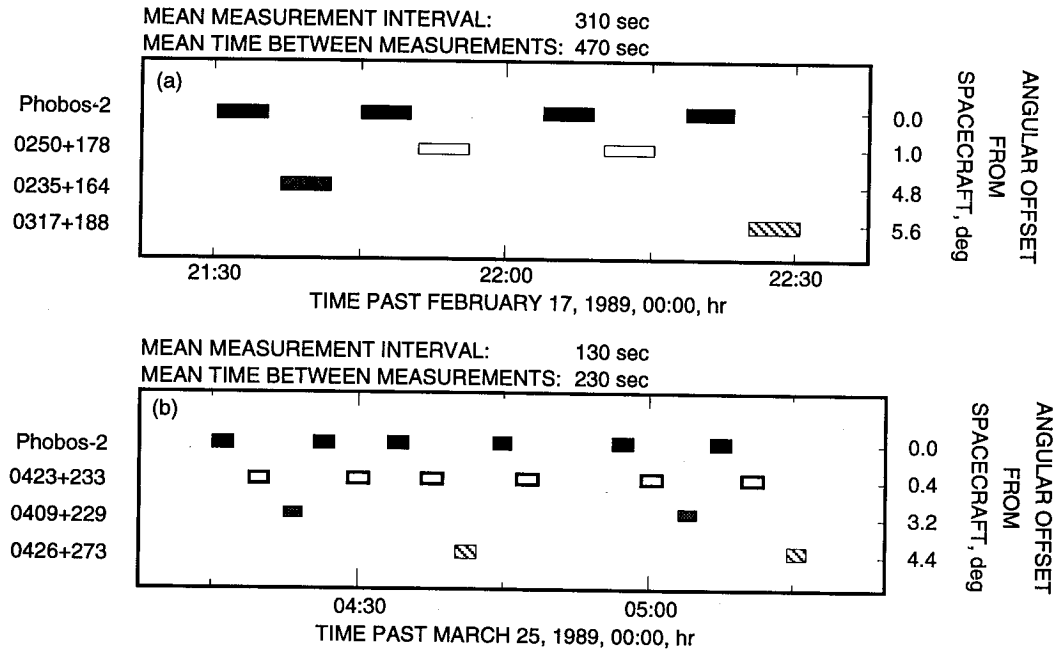

Fig. 4. Observation sequence: (a) February 17, 1989, and (b) March 25, 1989. Intervals of VLBI data acquisition for each source are shown by the horizontal bars.

Table 1. PHOBOS frame-tie error sources.

Error source	Magnitude	Notes
Thermal noise	Spacecraft, 0.18 nsec Quasar Wide-spanned bandwidth, 0.05 nsec Narrow-spanned bandwidth, 0.15 nsec	Approximate—sigmas are computed for each point during observable processing (see Appendix A)
Spacecraft orbit	February 17, 5.5 km March 25, 0.6 km	Spacecraft relative to Mars (See Footnote 7)
Planetary ephemeris	≈ 3 km	Mars relative to Earth orbit (See [6])
Zenith troposphere		
Constant	4 cm	(See [18] and Footnote 10)
Fluctuation at 1000 sec	1 cm	(See [19])
Ionosphere (Faraday calibration error)		
Time dependence	$0.5\sqrt{\Delta t/1000}$ nsec	See Appendix B
Bias	10 percent of calibration	
Solar plasma	~ 0.1 nsec	(See [21])
Instrumental bias	Goldstone–Madrid, 0.39 nsec Goldstone–Canberra, 0.10 nsec	(See Appendix A)
Quasar position	15 nrad (each component)	Source structure
Inertial station locations	20 cm (each component)	

IV. VLBI Measurement Sensitivity and Error Sources

A. Data Sensitivity

Following Finger and Folkner [2], the relation between the planetary and radio-frame positions of a body is assumed to be a rotation of coordinates having the form

$$\vec{r}_R = \vec{r}_P - \vec{A} \times \vec{r}_P$$

where $\vec{r}_P$ is the position in the planetary frame, $\vec{r}_R$ is the position in the radio frame, and $\vec{A}$ is a vector of small rotations ($|\vec{A}| \ll 1$). If the positions of a body are independently determined in both frames, the frame-tie vector $\vec{A}$ can be computed.

In the present case, the position of the Phobos-2 spacecraft is known in the planetary frame, and the PHOBOS VLBI data measure components of its angular position in the radio frame. The sensitivity of the VLBI delays to the frame-tie rotation vector is described below.

For the purposes of this discussion, the VLBI delay for the spacecraft is approximated by the time required for an electromagnetic wave transmitted by the spacecraft to traverse a distance in free space equal to the instantaneous offset in the locations of the two stations in the direction of the spacecraft geocentric position vector. That is, if $\hat{S}_R$ is a unit vector along the Earth-to-spacecraft line in the radio frame, the observed delay is

$$\tau_{obs} = \frac{\vec{B}}{c} \cdot \left(\frac{\vec{r}_R}{r} \right) = \frac{\vec{B}}{c} \cdot \hat{S}_R$$

where $\vec{B}$ is the baseline (i.e., vector separation of the two stations) in the radio frame and c is the speed of light.

The modeled delay is obtained from the previous equation by writing $\hat{S}_R$ as a function of the rotation vector $\vec{A}$ and the unit vector $\hat{S}_P$ but expressed in planetary frame coordinates:

$$\tau_{model} = \frac{\vec{B}}{c} \cdot \left(\hat{S}_P - \vec{A} \times \hat{S}_P \right)$$

Nominally, the rotation vector is assumed to be zero, so the modeled delay is

$$\tau_{model} = \frac{\vec{B}}{c} \cdot \hat{S}_P$$

and the delay residual (observed minus modeled) can be written as

$$\Delta\tau = \frac{\vec{B}}{c} \cdot \left(\hat{S}_R - \hat{S}_P \right) = -\frac{\vec{B}}{c} \cdot \left(\vec{A} \times \hat{S}_P \right)$$

Since it is assumed that $|\vec{A}| \ll 1$, $\hat{S}_P$ can be replaced by $\hat{S}_R$, so to first order,

$$\Delta\tau = -\frac{\vec{B}}{c} \cdot \left(\vec{A} \times \hat{S}_R \right) \tag{1}$$

The cross-product is given in terms of the components of the rotation vector $\vec{A}$ as

$$\vec{A} \times \hat{S}_R = \begin{bmatrix} 0 & -A_3 & A_2 \\ A_3 & 0 & -A_1 \\ -A_2 & A_1 & 0 \end{bmatrix} \hat{S}_R$$

From Eq. (1), it is clear that the delay residual depends only on the rotation component which is in the plane of the sky (POS). The POS is orthogonal to $\hat{S}_R$ (the Earth–spacecraft line of sight), so the relation of the delay residual to the rotation vector takes the form

$$\Delta\tau = -\vec{\tau}_{POS} \cdot \left(\vec{A}_{POS} \times \hat{S}_R \right) \tag{2}$$

where $\vec{A}_{POS}$ is the POS component of $\vec{A}$. The vector $\vec{\tau}_{POS}$ is also in the POS and is in the direction of the projection of the station baseline, i.e.,

$$\vec{\tau}_{POS} = \frac{1}{c}\left[\vec{B} - \left(\vec{B} \cdot \hat{S}_R\right)\hat{S}_R\right]$$

The rotation vector can be represented in terms of small increments in right ascension and declination as

$$\vec{A}_{POS} = -\Delta\delta\ \hat{u} + \Delta\alpha \cos\delta\ \hat{v}$$

The quantities α and δ are the right ascension and declination of the source, and the unit vectors $\hat{u}$ and $\hat{v}$ lie in the POS, with $\hat{u}$ in the direction of increasing right ascension (RA) and $\hat{v}$ in the direction of increasing declination (DEC) (Fig. 5).

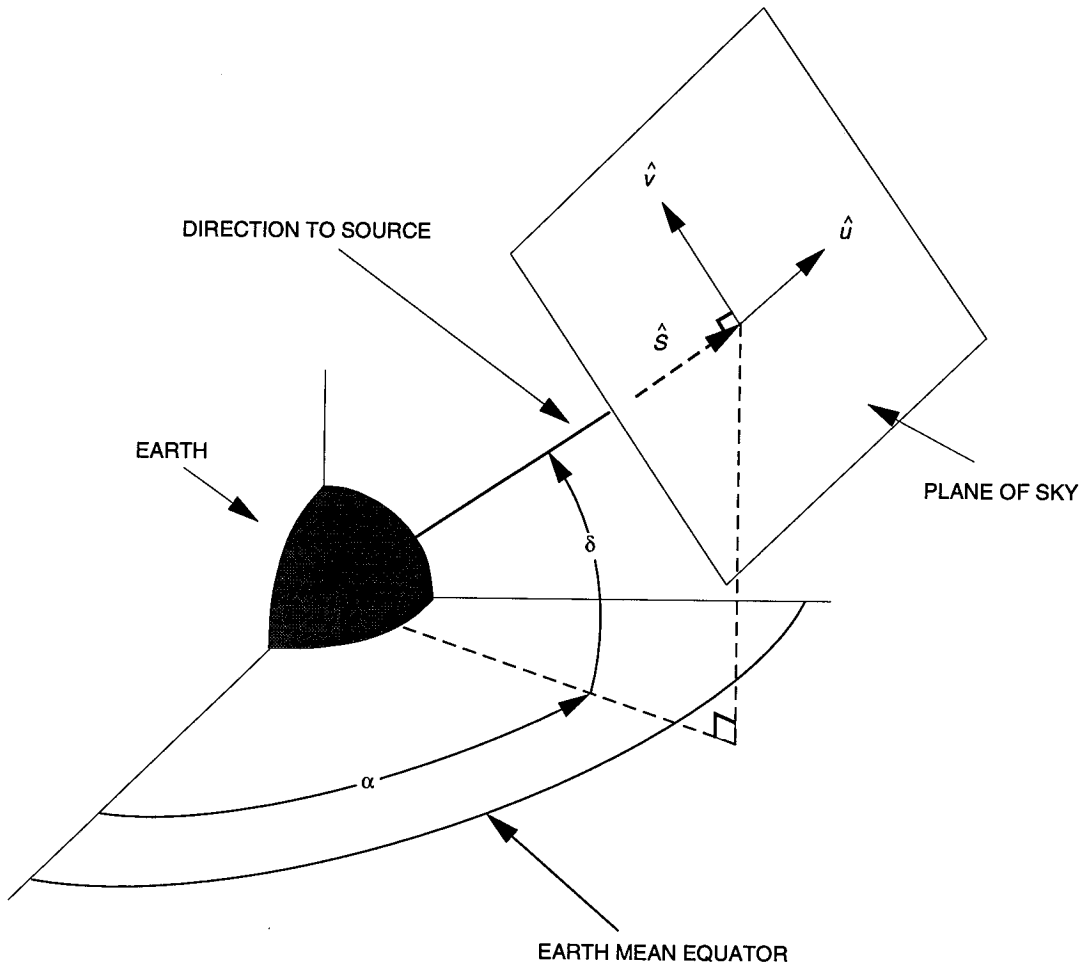

Fig. 5. Plane-of-the-sky coordinates.

A single delay measurement on a single baseline is sensitive only to that portion of $\vec{A}_{POS}$ which is orthogonal to $\vec{\tau}_{POS}$. With VLBI measurements on one baseline, some sensitivity to the second component of $\vec{A}_{POS}$ (in the POS and parallel to the projected baseline) is obtained with delay measurements separated in time so that Earth rotation causes the orientation of the projected baseline $\vec{\tau}_{POS}$ to change. The changes in projected baselines during the PHOBOS passes were mainly in length, not orientation (see Fig. 6), and the sensitivities to this rotation component are 30 to 40 times weaker than for the orthogonal

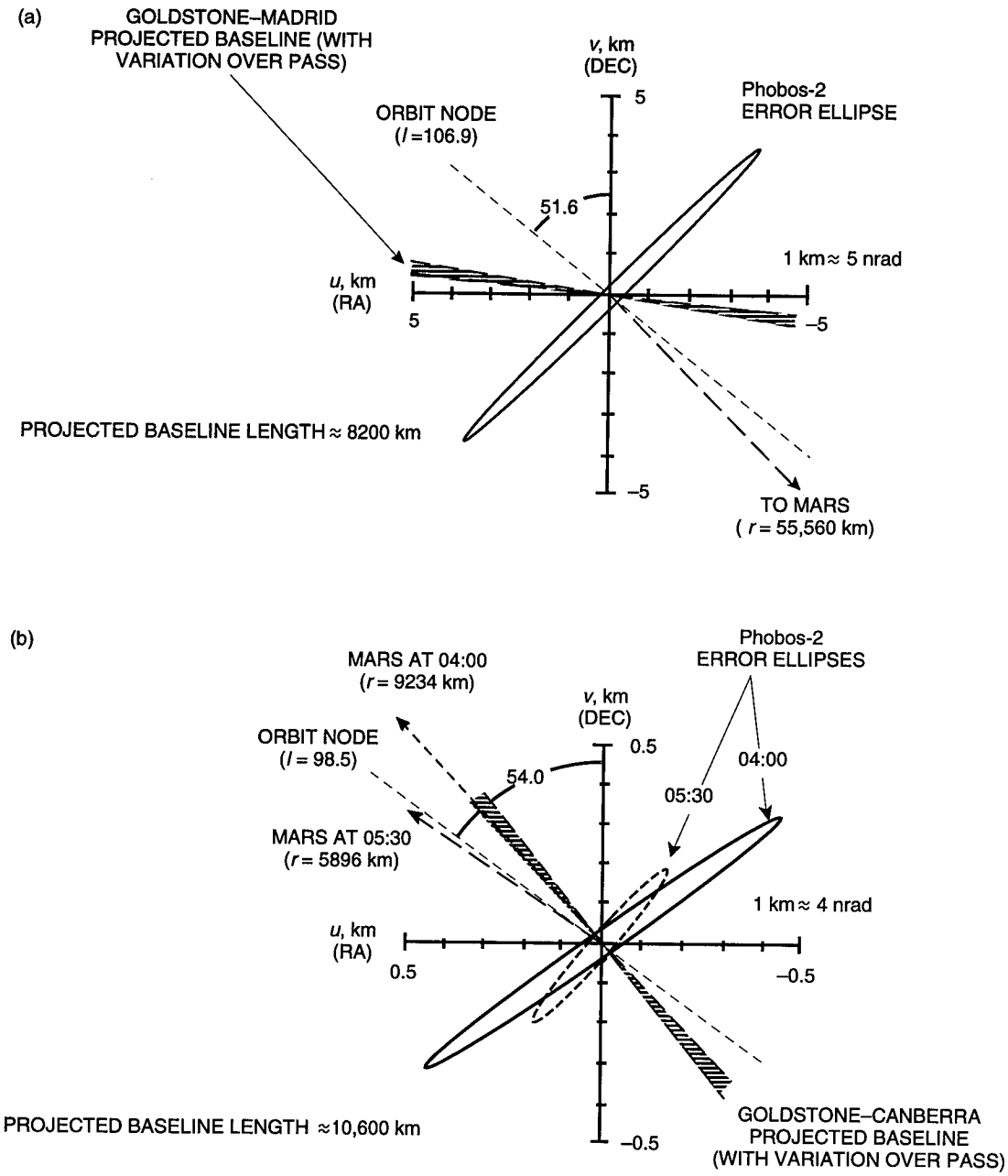

Fig. 6. Phobos-2 orbit errors in the plane of sky are represented by 1-σ error ellipses: (a) February 17, 1989, and (b) March 25, 1989. The projection of the station baseline is also shown. Only the component of the orbit error in the direction of the projected baseline affects the frame-tie parameter estimates. The orbit error for the March 25 pass is an order of magnitude smaller than for the February 17 pass.

component. A more accurate determination of the collinear component can be made by using data from a second baseline for which the projection on the POS has a large component orthogonal to the original $\vec{\tau}_{POS}$. A precise determination of the third component of $\vec{A}$, the rotation about the normal to the POS, would require an additional observation when the Earth–spacecraft line of sight was offset in angle by about 90 deg from its original direction.

The longest baselines for the first PHOBOS pass are approximately 8000 km in length, and mostly in the equatorial plane. The baseline for the second pass is about 10,000-km long, and has a large component

perpendicular to the equatorial plane. Together, the two passes provide baseline projections on the POS ($\vec{\tau}_{POS}$) which are large and have a large orthogonal component. But the motions of Earth and Mars between passes changed the orientation of the Earth–spacecraft line of sight by only 20 deg. Consequently, the PHOBOS data can provide accurate estimates of only two of the three rotation components.

B. Measurement Error Sources

The VLBI time delays are not just the differential signal arrival times at the two stations plus thermal noise, but include path delays due to media (ionosphere, troposphere, and solar plasma), instrumental phase response, and clock offsets, which are imperfectly known a priori. Furthermore, the delay models contain errors due to inaccuracies in spacecraft trajectory, Earth and Mars ephemerides, station locations, Earth orientation, and radio source positions. All of these effects have the potential to cause significant deviations in the residual delay, which in turn could cause errors in the frame-tie parameter estimates. The treatment of thermal noise, media, instrument, and clock effects in the process of obtaining the observed delay from the raw data is described in Appendix A. The important characteristics of both measurement and model errors as they pertain to the determination of the frame-tie parameters are summarized in Table 1.

1. Thermal Noise. Data weighting was based on estimates of the delay uncertainty from system noise obtained for each data point during postcorrelation processing (there is one data point for each observation interval on each source for a total of 22 delay measurements [see Fig. 4 and Section IV in Appendix A]). System noise effects in delay depend both on the signal strength and the range of frequencies that are sampled (the spanned bandwidth). For the spacecraft, with a usable bandwidth of about 30 MHz, the 1-σ delay uncertainty was typically about 0.2 nsec. Quasar delays were obtained for two different bandwidths—one set included measurements over the total spanned bandwidth of about 70 MHz and the other used essentially the same bandwidth as the spacecraft. The delay standard deviation from system noise for the widest spanned bandwidth was on the order of 0.05 nsec. For the narrow bandwidth, the delay uncertainty increased to 0.2 nsec. Solutions were obtained for each set of quasar delays separately, in combination with spacecraft delays, as a check on instrumental phase effects. (Note that a measurement error of 0.1 nsec corresponds roughly to an angular error of 3–4 nrad.)

2. Spacecraft Orbit. Since the VLBI data actually measure the angular offset between the quasars and the spacecraft, the frame tie can be achieved only if the a priori knowledge of the spacecraft position relative to Mars is sufficiently accurate. Phobos-2 spacecraft orbit estimates were obtained from the Navigation Systems Section. T. McElrath provided preliminary spacecraft trajectories in EME50 Cartesian coordinates relative to the DE118 planetary ephemeris, as well as covariances of errors in the spacecraft state estimates at the beginning of each pass.[5] Refined trajectories and covariances from orbit determination processing incorporating additional data were provided by J. P. Berthias.[6] The trajectories and covariances were transformed from EME50 coordinates to the Earth mean equator and equinox of J2000 (the DE200 system) by applying the rotation matrix given by E. M. Standish [6].

For the February 17, 1989, pass, the spacecraft was in a highly elliptic orbit with eccentricity of 0.8 and a period of 3.6 days. On March 21, 1989, it entered a nearly circular orbit with a period of 7.66 hr, which kept it close to Phobos (the mean distance from the satellite on March 25 was about 275 km). The data sets used for trajectory determination included instantaneous range rates derived from two-way C-band Doppler acquired by the Soviet network, two passes of two-way Doppler (C-band up,

[5] T. McElrath, personal communication, Navigation Systems Section, Jet Propulsion Laboratory, Pasadena, California, 1989.

[6] J.-P. Berthias, personal communication, Navigation Systems Section, Jet propulsion Laboratory, Pasadena, California, October 1990.

L-band down) from the DSN,[7] and, for the March 25 orbit, measurements of the relative angular position of the spacecraft and Phobos derived from onboard imaging.[8]

The accuracy of the estimated orbits is represented by the 1-σ error ellipses for the projection of the Phobos-2 Mars-relative position onto the plane of sky (Fig. 6). The shape and orientation of the error ellipses indicate that the dominant uncertainty is in the orbit angular orientation about the Earth–spacecraft line of sight, which is typical of orbits determined primarily from Doppler data.

The magnitude of the orbit uncertainty depends on several factors, including the accuracy of the data, the length of the data arc, and the orbit shape and orientation. The orbit accuracy for the pass on March 25, about 500 m, is an order of magnitude smaller than the several-kilometer uncertainty for the February 17 pass. Favorable orbit geometry for the second pass further reduces the effect of orbit error on the frame-tie estimates. These trajectory uncertainties correspond roughly to 15 nrad and <1 nrad in geocentric angular position for the first and second pass, respectively.

3. Planetary Ephemeris. Uncertainty in the DE200 positions of Mars and the Earth are described by a covariance matrix on the errors in the estimated orbital elements.[9] Included in this covariance are contributions due to a common angular offset of the orbits of Earth and Mars relative to the actual equator and equinox of the year 2000. It is this common angular orientation offset of the planetary and radio reference frames that is to be determined by the PHOBOS VLBI data, so the planetary ephemeris error model should reflect only the relative error in the positions of Earth and Mars. A covariance matrix for only this component of the error was obtained by statistically combining the a priori DE200 covariance with another covariance in which the sigmas on the parameters describing the orientation of the orbit of the Earth were essentially zero, and other orbit parameters were unconstrained. The 1-σ error ellipses for the resulting Earth–Mars direction uncertainty are shown in Fig. 7.

The ecliptic longitude of Mars relative to Earth's perihelion, and the inclination of the orbit of Mars to the ecliptic, have been determined from Viking lander range data [17]. The direction of the Earth–Mars line referenced to the orbit of the Earth is known to an uncertainty of 3 km (15 nrad) or better.

4. Troposphere. Tropospheric delay calibrations are computed using a seasonal model [18]. The calibration error is modeled as a constant offset in zenith troposphere delay at each site with a standard deviation of 4 cm.[10] The zenith uncertainty is mapped to the proper elevation angle using the standard mapping function (approximately $1/\sin\gamma$, where γ is the elevation angle). At the lowest elevation angles ($\gamma \approx 22$ deg), the delay uncertainty at one station is about 11 cm or 0.4 nsec. The troposphere error in the delay differenced between sources separated in elevation angle by 1 deg is nearly 60 times smaller (0.2 cm, or less than 0.3 nrad).

The magnitudes of the delay error to be expected from fluctuations in the wet troposphere delay on time scales corresponding to the time between measurements ($\approx$ 200–500 sec) and the duration of a pass ($\approx$ 1 hr) are taken from Fig. 2 of [19], which is based on the assumption of Kolmogorov turbulence, with parameters adjusted to agree with variations measured by water vapor radiometers at the DSN sites. This model predicts variations of several millimeters on time scales of a few minutes, and about 1 cm over the pass at an elevation of 20 deg.

---

[7] J.-P. Berthias, "Analysis of the Phobos-2 Radiometric Data Set," JPL Interoffice Memorandum 314-6 1129 (internal document), Jet Propulsion Laboratory, Pasadena, California, March 1990.

[8] J.-P. Berthias, October 1990, op. cit.

[9] E. M. Standish, personal communication, Navigation Systems Section, Jet Propulsion Laboratory, Pasadena, California, 1991.

[10] S. E. Robinson, "Errors in Surface Model Estimates of Zenith Wet Path Delays Near DSN Stations," JPL Interoffice Memorandum 335.4-594 (internal document), Jet Propulsion Laboratory, Pasadena, California, September 1986.

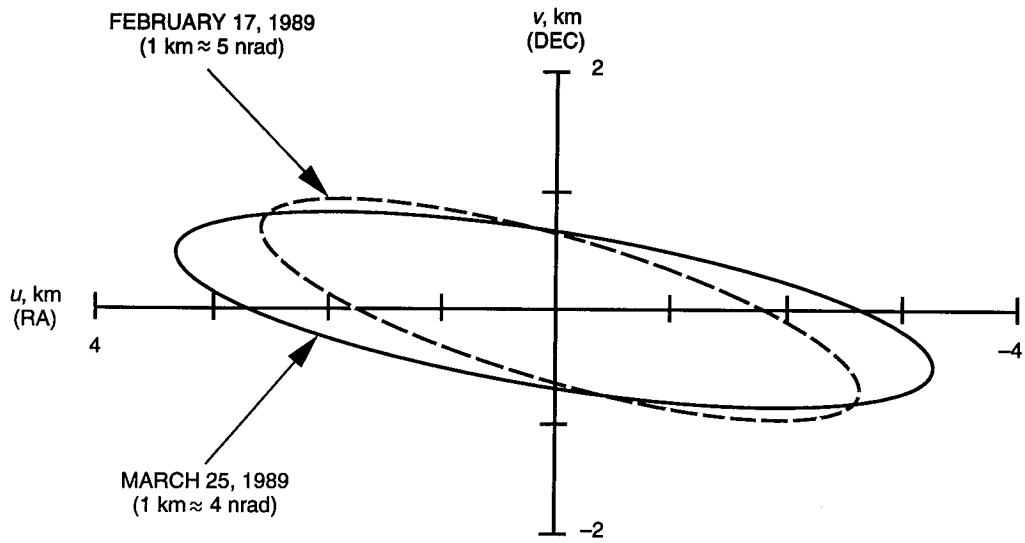

Fig. 7. Ephemeris DE200 error in the plane of sky (Mars relative to Earth–Moon barycenter orbit).

5. Ionosphere. Estimates of signal delays due to propagation through charged particles in the ionosphere were provided by the Tracking System Analytic Calibration Group. These estimates were based on measurements at each DSN site of the ionospheric delay of the signal from a geosynchronous Faraday beacon satellite [20]. To obtain delays along other ray paths, it is necessary to use a model for the temporal and spatial distribution of the ionosphere to map the measured ionosphere delay to the direction of other radio sources. The ionosphere mapping error is a major source of uncertainty in the ionosphere delay calibrations.

It is expected that the error in the ionosphere delay calibrations differenced between the spacecraft and quasar will depend to some extent on the apparent angular separation—the smaller the angle between the lines of sight, the closer together the ray paths through the ionosphere. For the small spacecraft–quasar separation angles of the PHOBOS data (in the range 0.4–5.6 deg), the time interval between measurements is also important. Earth rotation causes the position at which the ray path traverses the ionosphere to move in longitude at a rate of about 100 km in 5 min, whereas an angular source separation of 1 deg is equivalent to a position offset of approximately 10 km.

Because of uncertainties in assessing the spatial variability of the ionosphere over angular scales of many degrees, a subset of the quasar delay data was used to obtain the nominal frame-tie solution. The reduced quasar data set contains observations only of the quasar with the smallest angular separation from the spacecraft on each day (1.0 and 0.4 deg for the February 17 and March 25 passes, respectively). The main calibration errors were then modeled as temporal rather than spatial variations. In determining the frame-tie parameters, offsets of station clock epochs and rates were estimated for each pass with large a priori uncertainties (1-σ of 1 msec in epoch and 10^{-9} in rate). This essentially eliminated estimate errors due to linear time variations of the calibration error. An analysis of Magellan S- and X-band data (Appendix B) showed that the deviation of the calibration error from a linear model had the form of a random walk. In the estimation process, the amplitude of the random walk was adjusted to yield a reduced χ^2 of 1.

An indication of the remaining sensitivity to calibration error was obtained by assessing the effect on the frame-tie parameter estimates of an error in Faraday calibration scaling. The a priori uncertainty for the calibration scaling was set to 10 percent of the calibration. This translates to approximately 2 cm or less in the delay difference between the spacecraft and nearest quasar.

6. Space Plasma. Plasma-induced variances of delay measurement errors are derived from the structure function of plasma phase variations. With the assumption that the plasma is concentrated in a thin screen that passes through the center of the Sun and is perpendicular to the line of sight from the Earth to the radio source, the structure function of phase for a homogeneous and isotropic plasma takes the form

$$D_\phi(b) \equiv \langle [\Delta\phi_{plasma}(x+b) - \Delta\phi_{plasma}(x)]^2 \rangle$$

where $\Delta\phi_{plasma}(x)$ is the plasma phase delay for a ray path that crosses the thin screen at a distance x from the center of the Sun [23]. From the analysis of [21], the structure function $D(b)$ of quasar group delay fluctuations due to the charged particles of the solar plasma is

$$D(b) = \frac{2.5 \times 10^4}{f^4} \left(\frac{b}{V_{SW}}\right)^{1.65} (\sin SEQ)^{-2.45} \text{ nsec}^2$$

SEQ is the Sun–Earth–quasar angle in deg, b is the length of the projection of the baseline on the plane of sky (or equivalently the thin screen) in km, V_{SW} is solar wind speed in km/sec, and f is signal frequency in GHz. This structure function is based on the phase scintillation spectrum of [22], which is specified to be valid in the range of 20 to 100 solar radii, or about 5–30 deg in SEQ. For SEQ angles of 30–90 deg, the model slightly overestimates the phase scintillation spectrum. For the spacecraft delay, the structure function has the same form, but the value of b is taken as the separation between the lines of sight at the points of closest approach to the Sun, which is smaller than the projected baseline due to parallax.

Using the approach given in [23], it can be shown that the standard deviation $\sigma_{\Delta\bar{\tau}}$ of the plasma error in delay averaged over an interval T in sec is given by

$$\sigma_{\Delta\bar{\tau}} = \frac{\sqrt{2.5 \times 10^{-4}}}{f^2} \left(\frac{b}{V_{SW}}\right)^{0.825} (\sin SEQ)^{-1.225} G(\kappa) \text{ nsec}$$

where

$$\kappa \equiv T \left(\frac{b}{V_{SW}}\right)^{-1}$$

$$G(\kappa) = \left\{(2.65 \times 3.65 \times \kappa^2)^{-1} \left[(\kappa+1)^{3.65} + |\kappa-1|^{3.65} - 2\left(\kappa^{3.65}+1\right)\right]\right\}^{1/2}$$

For the March 25 geometry (projected baseline of 10,600 km and $SEQ = 64$ deg) with a solar wind speed of 400 km/sec, the delay standard deviation for an averaging time of 130 sec is 70 psec. The corresponding value for February 17 (8200-km baseline, $SEQ = 78$ deg, and $T = 310$ sec) is 42 psec.

The 1-σ error in the difference of two averaged delays separated in time by Δt is

$$\sigma_{\Delta^2\bar{\tau}} = \frac{\sqrt{2.5 \times 10^{-4}}}{f^2} \left(\frac{b}{V_{SW}}\right)^{0.825} (\sin SEQ)^{-1.225} F(\kappa, \Delta\kappa) \text{ nsec}$$

where

$$F^2(\kappa,\Delta\kappa) = 2G^2(\kappa) + \left(2.65 \times 3.65 \times \kappa^2\right)^{-1} \left\{ 2\left[|\Delta\kappa+1|^{3.65} + |\Delta\kappa-1|^{3.65} - 2|\Delta\kappa|^{3.65}\right] \right.$$

$$- \left[|\kappa+\Delta\kappa+1|^{3.65} + |\kappa+\Delta\kappa-1|^{3.65} - 2|\kappa+\Delta\kappa|^{3.65}\right]$$

$$\left. - \left[|\kappa-\Delta\kappa+1|^{3.65} + |\kappa-\Delta\kappa-1|^{3.65} - 2|\kappa-\Delta\kappa|^{3.65}\right] \right\}$$

$$\Delta\kappa \equiv |t_2 - t_1| \left(\frac{b}{V_{SW}}\right)^{-1}$$

For time intervals up to 1 hr, the model standard deviations for the difference of averaged plasma delays are less than 0.1 nsec.

For *SEQ* near 90 deg, measured spectral densities vary by up to 2 orders of magnitude [22], so that the plasma structure function given above may be too large or too small by a factor of 10. The corresponding upper limit for the PHOBOS plasma delays is about 0.3 nsec.

7. Instrumental Bias. The difference between the recorded spectra of the spacecraft and quasars may cause spacecraft delays to be biased relative to those of the quasars. The sampled spacecraft signal consisted of a series of discrete, coherent tones. For the quasars, the recorded spectrum was composed of several narrow "windows" (commonly referred to as "channels"), each consisting of white noise over a 2-MHz bandwidth (Fig. 8). The overall bandwidth of the sampled quasar spectra was much larger than that of the spacecraft signal—approximately 70 MHz versus 30 MHz. Estimates of the resulting delay bias errors are 0.39 nsec on the Goldstone–Madrid baseline and 0.10 nsec for Goldstone–Canberra. These values for the delay bias uncertainties are obtained from postcorrelation processing, as described in Appendix A.

8. Quasar Position. Source coordinates were taken from the IERS celestial reference frame RSC(IERS) 91 C 01 [8]. The accuracy with which the position of any given source is tied to this frame depends on several factors, including the number of observations available, observation frequencies, signal strength, and source structure. Generally, quasar positions are known with an accuracy of <5 nrad. The accuracy for the PHOBOS sources is not this good. With only a single exception (0235+164), the PHOBOS sources have only recently been added to the catalog, and repetitive observations that would provide a check on the consistency of the position determinations are not available.

Although the formal uncertainties in PHOBOS source positions are 6 nrad or less, the actual errors are almost certainly larger. The signal strengths of the quasars within 1 deg of the Phobos-2 spacecraft are fairly low. This could be an indication that the sources are not compact but have significant structure that might affect repeatability of the position estimates. Furthermore, the astrometric measurements were made at S- and X-bands while the frame-tie data were taken at L-band, so the position used in the frame-tie determination may be in error due to differences in structure at the different observing frequencies. For these reasons, the standard deviation of the quasar positions is conservatively taken to be 15 nrad in both right ascension and declination.

9. Inertial Station Locations. Locations of the radio antennas are given in the IERS Terrestrial Reference Frame (TRF) 1988.0 [8]. Continental drift was not modeled, so this error is included in the station location standard deviations. The size of the continental drift error is taken as the maximum value given by the AM0-2 plate motion model (7 cm or less [24]). Uncertainties of the crust-fixed locations (10 cm) are based on the accuracy of the determination of the geocenter [25,26]. The orientation of IERS TRF 1988.0 in inertial space is described by Earth polar motion, universal time, and the direction of the celestial pole. The polar motion and universal time calibrations used were consistent with the

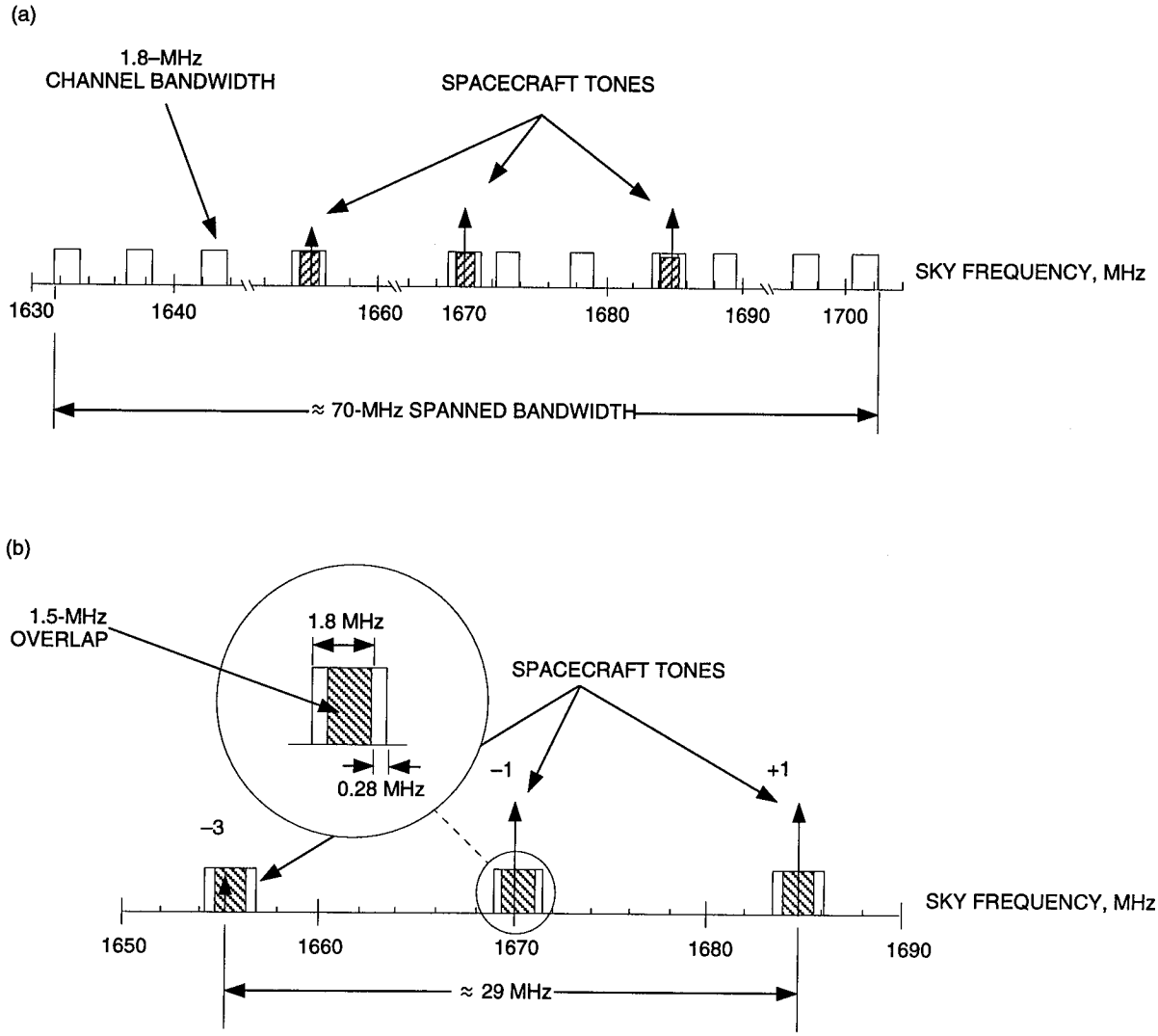

Fig. 8. VLBI channel configuration: (a) all channels and (b) spacecraft channels.

IERS celestial and terrestrial frame definitions at the 6-cm level [8]. The direction of the celestial pole was modeled by the 1980 IAU nutation model, which is consistent with the IERS frame definitions at the 6-cm level [8]. The uncertainty in inertial station locations due to errors in crust-fixed position and Earth orientation were combined and treated as "equivalent" errors in station locations with a standard deviation of 20 cm per component.

V. Results

A. Reference Solution

Figure 9 gives delay residuals relative to an a priori model. Drifts on the order of a few parts in 10^{13} caused by station clock rate offsets and uncalibrated ionosphere have been removed by fitting all residuals from a given baseline to a linear polynomial. The spacecraft delay residuals are indicated by filled circles, those for the primary quasars by open circles, and for the secondary quasars by triangles. The "primary quasar" is the one with the smallest angular separation from the spacecraft for each pass. The other

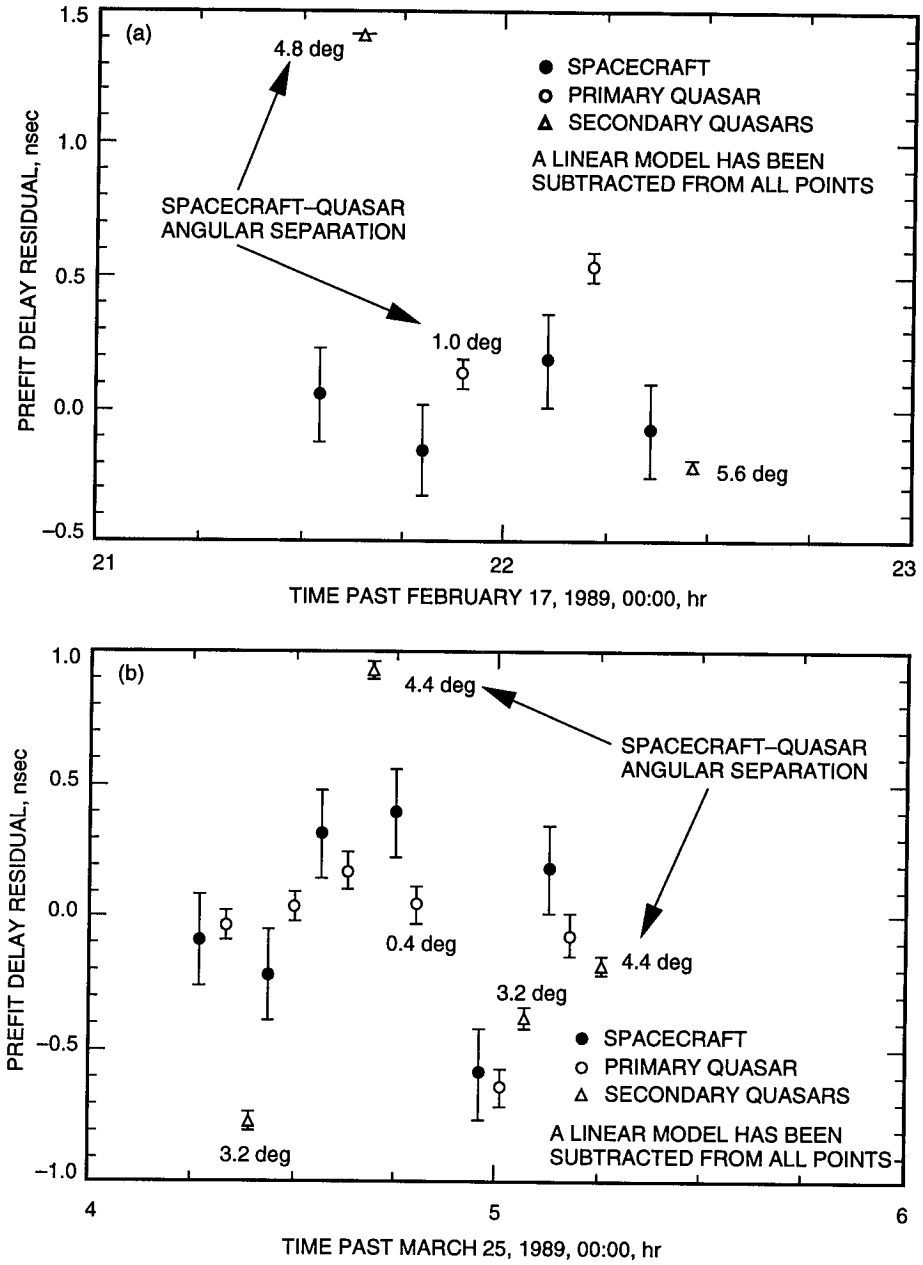

Fig. 9. Prefit delay residuals: (a) Goldstone–Madrid and (b) Goldstone–Canberra.

sources are referred to as "secondary quasars." The a priori model assumes the offsets of the planetary frame relative to the radio frame are zero; a nonzero offset causes a bias in the difference of the spacecraft and quasar delays.

The maximum difference between the spacecraft and quasar residuals is about 1.6 nsec for both passes. Residuals of this magnitude could be produced by errors of about 60 nrad in spacecraft angular position along the projection of the baselines on the plane of sky. However, for those cases in which a spacecraft observation was immediately followed by an observation of the primary quasar, the difference in delay is much smaller—always less than 0.5 nsec. This is consistent with the hypothesis that the 1.6-nsec offsets are due to model errors that are not canceled in the difference between the spacecraft and secondary quasars. Furthermore, the scatter in the residuals is larger than the 1-σ system noise error (indicated

by error bars), and significant changes in delay residuals are seen between successive points on a single source—the largest is 1.2 nsec between the spacecraft points at 4:45 and 4:58 for the March 25 pass. These effects are most likely due to error in the Faraday calibration of the ionospheric delays.

A noise model for the measurement error due to uncalibrated ionosphere was devised as described in Appendix B. The resulting structure function for the calibration error relative to a linear variation has the form of a random walk. That is, the error for measurement $i+1$ is related to that of measurement i by

$$\tau^I_{i+1} = \tau^I_i + w_i$$

and the a priori standard deviations of the w_i have the form

$$\sigma_w(i) = C\left(\frac{t_{i+1} - t_i}{1000}\right)^{1/2}$$

Here, C is the a priori standard deviation for points separated in time by 1000 sec. Analysis of Magellan S-/X-band (2.3 and 8.4 GHz, respectively) data yielded an initial value for C of 0.26 nsec at the PHOBOS frequency.

The w_i(i = 1 to N-1 for N data points) were then taken to be additional (correlated) measurement noise. The value of C was adjusted to 0.5 nsec to give a weighted sum of squares of postfit residuals near the expected value. The initial error τ^I_1 was not included, since this constant delay offset can be absorbed into the clock epoch correction (see below in this section).

Measurements from the secondary quasars were not included in the reference fit because the errors in the differenced ionosphere delay calibrations were expected to be several times larger at separation angles of 3.2–5.6 deg than at 1 deg or less. Although the random walk model strictly applies only to successive observations of the same source, it was assumed to accurately represent the differential delay error between the spacecraft and primary sources as well.

Data for baselines including the Jodrell station were not used in the reference fit. Jodrell is at a significantly higher latitude than the DSN stations, and the mapping of the Faraday calibration to the ionospheric pierce point may not be as accurate as for the DSN data.

Clock epoch offset and rate for each baseline were estimated to account not only for actual clock offsets, but also for any errors that are common to the spacecraft and quasar delays and which vary over the pass approximately linearly in time. Solving for these clock model parameters provides error cancellation even though the spacecraft and quasar delays were not explicitly differenced.

The delays were weighted with the inverse of the delay variances obtained during postcorrelation processing (Appendix A). These statistics mainly reflect the delay uncertainties due to system noise. For the reference solution, the quasar delays were produced from phases measured in 14 channels, each with a bandwidth of approximately 2 MHz, spread over 70 MHz (Fig. 8). The spacecraft delays utilize four channels for the February 17 pass and six for the pass on March 25, with a total spanned bandwidth of 29.4 MHz.

The remaining error sources were included via "consider" analysis [27]. That is, the errors in the estimates of the frame-tie parameters produced by 1-σ errors in the a priori value of each consider parameter were determined. The considered parameters were as follows:

(1) Spacecraft position and velocity at a specified epoch.

(2) Ephemeris correction parameters for the orbit of Mars relative to the orbit of the Earth (at the epoch of the ephemeris).

(3) Constant zenith troposphere calibration error for each station.

(4) Constant Faraday ionosphere calibration error in scale (each station).

(5) Spacecraft versus quasar instrumental biases (constants, modeled as a bias in spacecraft delay for each baseline).

(6) "Equivalent" station locations (includes crust fixed positions, continental drift, and Earth orientation).

(7) Constant errors in quasar positions.

The PHOBOS data are sensitive to only two of the three components of the frame-tie rotation vector, so the solutions are best presented in a plane orthogonal to the major principal axis of the error ellipsoid. Orthogonal axes P_1, P_2 in this plane are defined such that P_1 is along the intersection with the nominal inertial reference plane (DE200 Earth mean equator of J2000). This coordinate system is shown in Fig. 10, and the two well-determined components of the rotation vector along with their 1-σ error ellipse are given in Fig. 11(a). The P_1, P_2 axes are closely aligned with the POS vectors $-\hat{u}$ and $+\hat{v}$ for some effective Mars right ascension and declination determined by the data. The right ascension of Mars for the two passes differed by about 22 deg, and the declination by 5 deg, so this alignment of axes is only approximate. The minor axis of the error ellipsoid is nearly orthogonal to the projection of the Goldstone–Canberra baseline on the POS.

For convenience of comparison with other frame-tie determinations, the solutions and error ellipses are also presented in terms of spacecraft right ascension and declination [Fig. 11(b)]. Again, these values are only approximate, for the reasons given above. The complete consider covariance on the components of the frame-tie vector $\vec{A}$ and the corresponding error ellipsoid are given in Tables 2 and 3. (Note that the consider covariance is the covariance on the estimates accounting for all error sources, including thermal noise and random walk calibration error.)

The reference solution is consistent with a frame offset of zero in the P_1, P_2 plane. A breakdown of the contribution of the individual error sources to the overall accuracy of the determination of these rotation components is shown in Fig. 12. The labels "February 17 Orbit" and "March 25 Orbit" denote Phobos-2 orbit errors, and "G/C" and "G/M" refer to the Goldstone–Canberra and Goldstone–Madrid baselines, respectively. The consider errors tend to align with either the semimajor or semiminor axes of the total error ellipse. Most of the error is due to the instrumental delay biases for the February 17 pass and to the uncertainty in the Phobos-2 orbit on this day. The uncertainties in the minor axis direction have a large contribution from errors in the position of Mars relative to Earth as given by DE200. There is also a significant error due to uncertainty in the quasar positions in the radio frame.

B. Solution Consistency

Several variations on the basic estimation scheme were tried to determine if the scatter in the solutions was consistent with the expected errors. The results below are for the following fits:

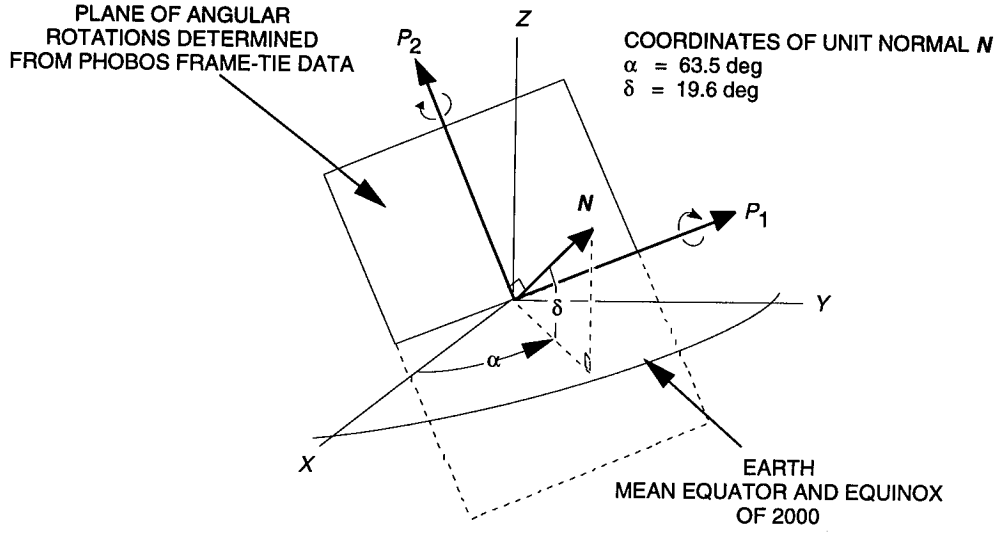

Fig. 10. PHOBOS frame-tie coordinates.

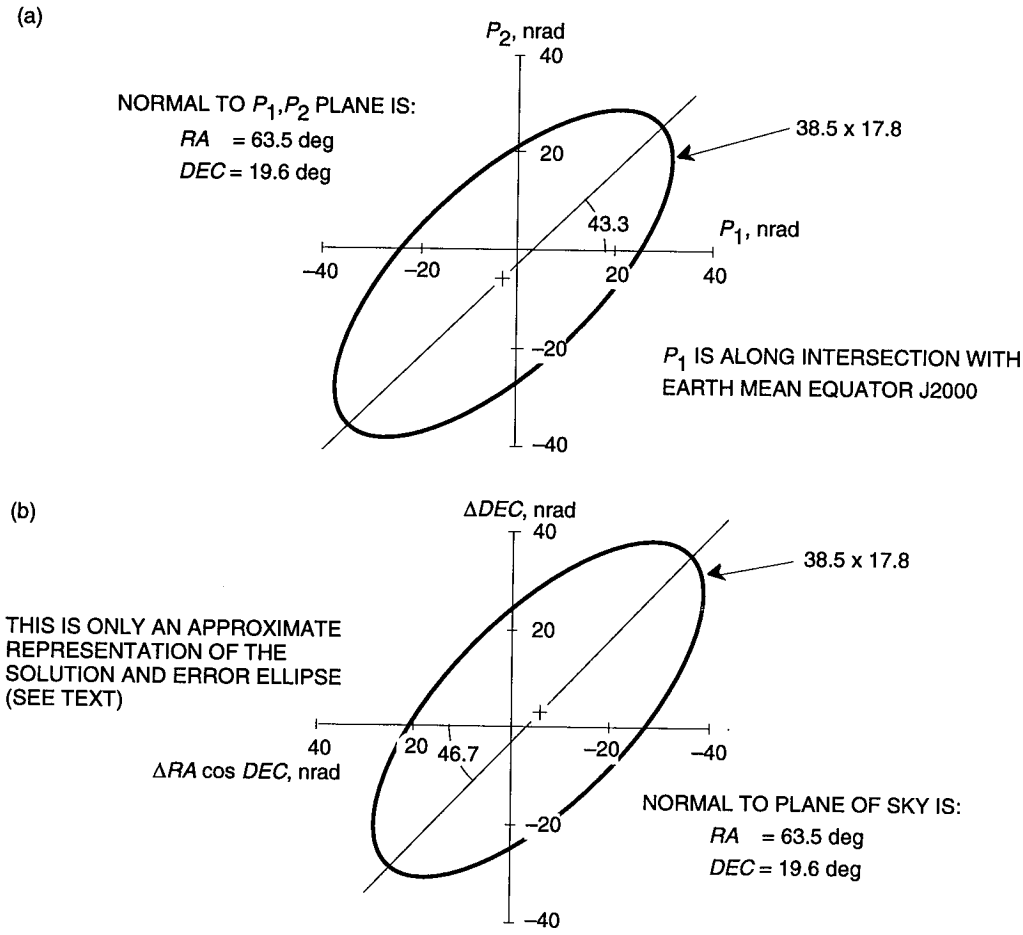

Fig. 11. PHOBOS frame-tie reference solution and error ellipse: (a) P_1,P_2 coordinates and (b) right ascension and declination.

(1) Madrid (DSS 63) replaced by Jodrell

(2) Quasar delays computed from phases in spacecraft channels only

(3) Delays from all quasars included in solution

(4) Case (3) without random walk ionosphere measurement noise

Solutions for these cases are shown with the reference solution in Fig. 13.

For fit (1), the data set is the same as for the reference solution except that Goldstone–Jodrell delays are used instead of those from the Goldstone–Madrid baseline. Comparison of these estimates with the reference solution potentially could reveal delay measurement errors due to differences in instrumentation between the DSN stations and the Jodrell station. Instrumental errors may occur if the manual phase calibration procedure fails, or if there are significant shifts in phase in spacecraft tones due to small scale phase variations with frequency. But the observables are also different because of other errors that are not the same at Jodrell and Madrid. For example, differences on the order of 0.1 nsec (about 4 nrad) are expected from system noise, and differences of several nanoradians could be caused by ionosphere calibration error in scale. The actual difference in solutions is 7 nrad, so there is no evidence of significant instrumental error.

For case (2), instrumental errors could cause the quasar delays to depend upon the specific channels used in obtaining the measured delays. Also, reducing the number of channels increases the system noise error in the delays. Again the estimates for this case are in good agreement with the reference solution.

Fits for cases (3) and (4) show the effect on the solutions of including the delays from the secondary sources, which are expected to have nanosecond-level errors due to uncalibrated ionosphere. For case (3), the a priori sigmas on the random walk ionosphere parameters were doubled (to 1 nsec in 1000 sec) to yield an acceptable weighted sum-of-squares (WSOS) for the postfit residuals. Doubling the sigmas produced only small increases in the uncertainties of the estimates. It is probably fortuitous that the

Table 2. Estimated J2000 Cartesian frame-tie vector $\vec{A}$ and consider covariance matrix.

Component	Solution, nrad	Consider covariance, nrad^2		
		A_1	A_2	A_3
A_1	61.1	89,285.29	180,220.16	72,333.97
A_2	131.1	—	368,556.02	148,959.86
A_3	58.8	—	—	60,993.31

Table 3. Frame-tie estimate and covariance referred to consider covariance principal axes.

Solution, nrad	Semiaxes, nrad	Unit principal axes in J2000 frame		
		a	b	c
−156.1	719.05091	0.41338401	−0.75676500	0.50637970
5.8	38.53070	0.84417073	0.11006405	−0.52465386
2.3	17.77020	0.34130548	0.64435444	0.68433758

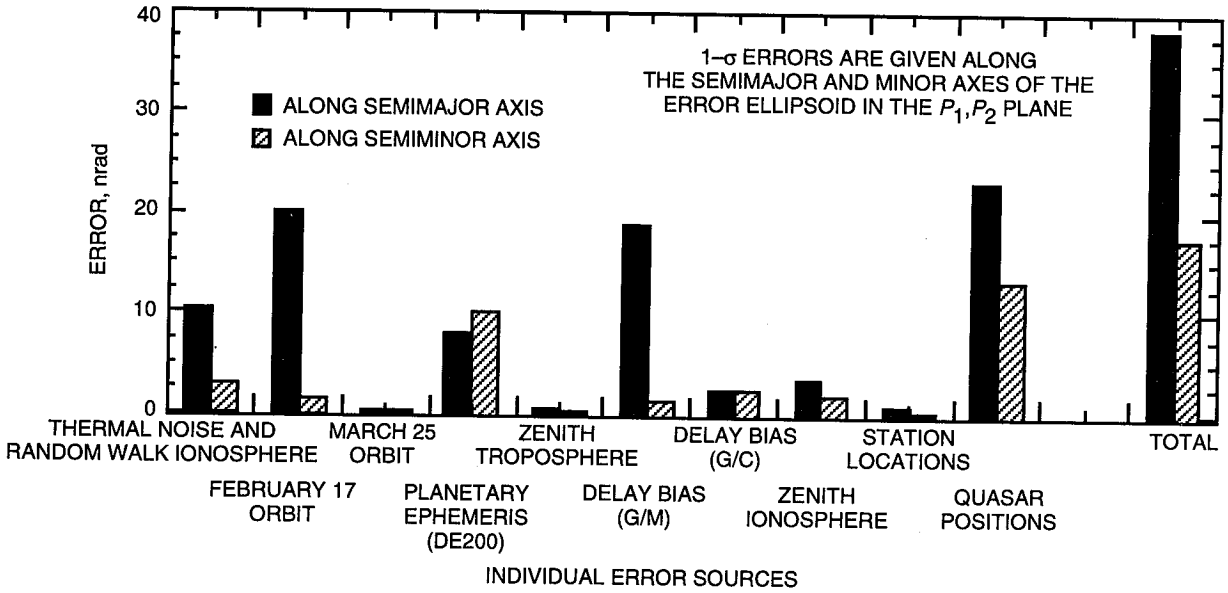

Fig. 12. PHOBOS frame-tie error summary.

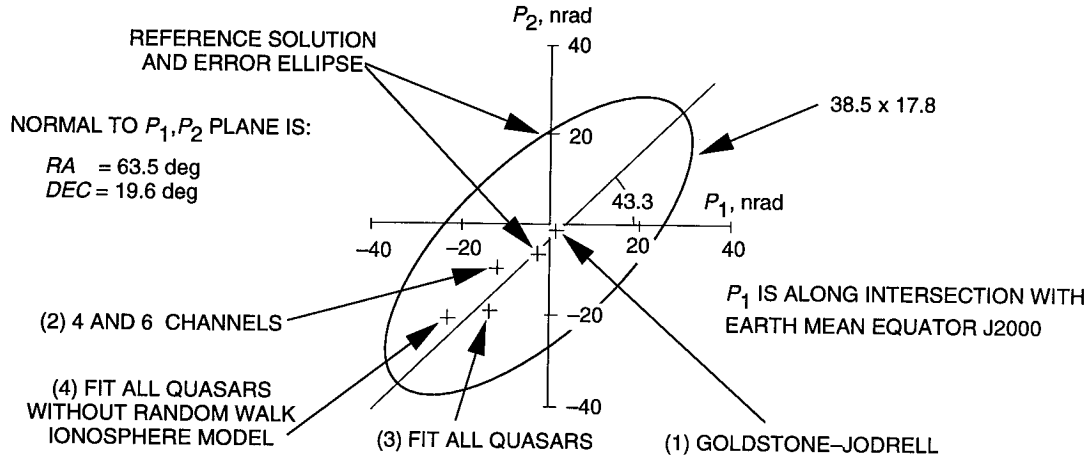

Fig. 13. PHOBOS frame-tie solution consistency.

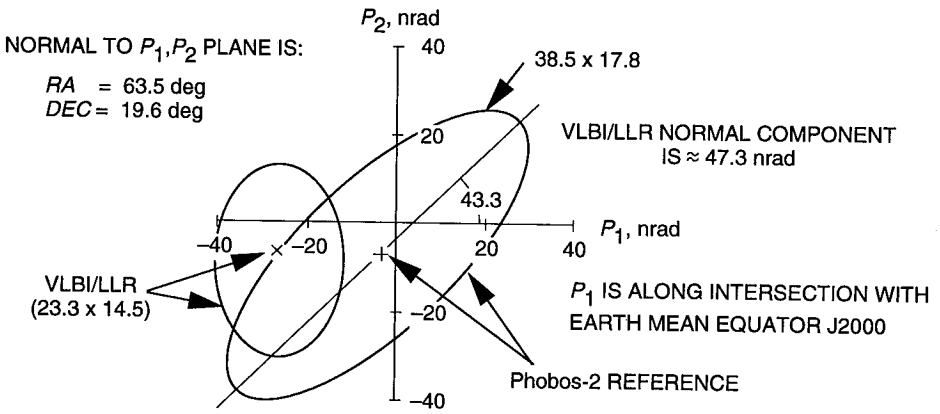

Fig. 14. PHOBOS frame tie versus VLBI/LLR.

case (4) result is consistent with other solutions; without the ionosphere contribution to the measurement noise, the WSOS of the postfit residuals was extremely large.

C. Comparison With Other Frame-Tie Estimates

Since the PHOBOS data provide accurate estimates of only two components of the small rotation vector relating the planetary and radio frames, these results cannot in general be compared with estimates presented as corrections to right ascension and declination. It is possible, however, to check the agreement with the three-component VLBI–LLR frame tie [2].

The VLBI–LLR frame tie was derived from a comparison of station location and Earth orientation parameter values based on DSN VLBI data with those obtained from lunar laser ranging data. Ground ties between the DSN stations, VLBI stations of the Crustal Dynamics Project, satellite laser ranging sites, and lunar laser ranging sites were also employed. The LLR data provide the tie to the planetary frame, as these data provide the location of the dynamical equinox to which the positions of the planetary ephemeris are referenced. The accuracy of the VLBI/LLR frame tie is about 15 to 20 nrad (Table 4).

The VLBI–LLR components in the PHOBOS P_1, P_2 frame with their corresponding error ellipse are shown in Fig. 14. The difference between the two solutions corresponds to about 0.7σ. The PHOBOS data are not sensitive to the third component, which, with a value of 47.3 nrad, is the largest of the three VLBI–LLR rotation parameter estimates.

Table 4. VLBI/LLR frame-tie referenced to Earth mean equator and equinox of J2000.

Component	Value, nrad	σ, nrad
A_1	5	15
A_2	−49	15
A_3	−19	25

VI. Conclusions and Future Activities

Two passes of VLBI data were acquired at the DSN from the Soviet Phobos-2 spacecraft while it was in Mars orbit. VLBI observations of quasars at small angular separations (1 deg or less) from the spacecraft were also included. These data are sensitive to the orientation of the Earth–Mars line of sight relative to the reference frame defined by the coordinates of selected extragalactic radio sources. Because the positions of Earth and Mars are well known within the frame of the planetary ephemeris, analysis of the VLBI measurements has yielded estimates of two components of the angular rotation relating the frame of JPL planetary ephemeris DE200 to the IERS radio frame. The 1-σ uncertainty in the frame-tie rotation components is 20–40 nrad, depending on direction.

The accuracy of the frame tie cannot be better than the internal consistency of either the planetary ephemerides or the radio source catalog. Relative positions of catalogued sources are stable to the order of 5 nrad [10]. The internal consistency of the planetary ephemeris is not as good. For example, Earth and Mars have uncertainties in their mean motions on the order of 1 nrad/yr [12].[11]

In the same way that the PHOBOS data measured the Earth–Mars direction in the radio frame, VLBI data acquired from the Magellan spacecraft are being used to measure the Earth–Venus direction with

[11] J. G. Williams, personal communication, Tracking and Applications Section, Jet Propulsion Laboratory, Pasadena, California, 1993.

an accuracy of 5 nrad.[12] The Magellan VLBI data cannot directly improve the frame-tie determination because the uncertainty in the position of Venus in the planetary frame is about 100 nrad. But these data can give precise information on the motions of Earth and Venus in the radio (inertial) frame. Future missions using planetary orbiters or landers with the capability of providing ranging data with meter-level accuracy, in addition to VLBI delay measurements, would enable additional opportunities to improve the frame tie. With differential VLBI delay accuracy comparable to the Magellan data, a frame-tie accuracy of 10 nrad or less should be achievable.

Acknowledgments

The Phobos-2 VLBI measurements were acquired in preparation for a high-accuracy frame-tie determination that would have employed VLBI data from a lander on the surface of the Mars' satellite Phobos. The principal investigators for the PHOBOS lander frame-tie experiment and their affiliations were Jacques Blamont (CNES), Vyacheslav Linkin (IKI) and Robert Preston (JPL/NASA). The authors would like to thank the following: Roger Linfield for his careful reading of several versions of this article and his helpful suggestions; Dave Fort for providing valuable consultations in processing the data on the DSN Block II correlator; Jim Border for help in generating spacecraft and correlator predicts; Tim McElrath and Jean-Paul Berthias for spacecraft trajectory estimates and the associated covariances; Brian Wilson and Titus Roth for providing ionosphere calibrations; the TEMPO and TSAC teams for providing Earth-orientation, troposphere calibrations and Faraday calibrations of ionosphere delays; and Jim Williams and Mark Finger for many helpful discussions and suggestions along the way.

References

[1] D. Jones, R. Dewey, C. Gwinn, and M Davis, "Mark III VLBI Astrometry of Pulsars," IAU Colloquium 131, *Radio Interferometry: Theory, Techniques, and Applications*, T. Cornwell, ed., Sicorro, New Mexico, 1990.

[2] M. H. Finger and W. M. Folkner, "A Determination of the Radio-Planetary Frame Tie From Comparison of Earth Orientation Parameters," *The Telecommunications and Data Acquisition Progress Report 42-109, vol. January–March 1992*, Jet Propulsion Laboratory, Pasadena, California, pp. 1–21, May 15, 1992.

[3] A. E. Niell, XX Newhall, R.A. Preston, G. L. Berge, D. O. Muhleman, D. J. Rudy, J. K. Campbell, P. B. Esposito, and E. M. Standish, "Relating the Planetary Ephemerides and the Radio Reference Frame," *The Telecommunications and Data Acquisition Progress Report 42-81, vol. January–March 1985*, Jet Propulsion Laboratory, Pasadena, California, pp. 1–8, May 15, 1985.

[12] Folkner et al., op. cit.

[4] XX Newhall, R. A. Preston, and P. B. Esposito, "Relating the JPL VLBI Reference Frame and the Planetary Ephemerides," *Proceedings of IAU Symposium 109, Astrometric Techniques*, H. K. Eichhorn and R. J. Leacock, eds., D. Riedel, pp. 789–794, 1986.

[5] T. P. McElrath and R. S. Bhat, "Determination of the Inner Planet Frame Tie Using VLBI Data," paper 88-4234, AIAA/AAS Astrodynamics Conference, Minneapolis, Minnesota, 1988.

[6] E. M. Standish, "Orientation of the JPL Ephemerides, DE200/LE200, to the Dynamical Equinox of J2000," *Astron. Astrophys.*, vol. 114, pp. 297–302, 1982.

[7] E. M. Standish, "The Observational Basis for JPL's DE200, the Planetary Ephemeris of the Astronomical Almanac," *Astron. Astrophys.*, vol. 223, pp. 252–271, 1990.

[8] *Annual Report for 1990*, International Earth Rotation Service, Observatoire de Paris, Paris, France, 1991.

[9] C. Hazard, J. Sutton, A. N. Argue, C. M. Kenworthy, L. V. Morrison, and C. A. Murray, "Accurate Radio and Optical Positions of 3C273b," *Natural Physical Science*, vol. 233, pp. 89–91, 1971.

[10] E. F. Arias, M. Feissel, and J.-F. Lestrade, "An Extragalactic Celestial Reference Frame Consistent With BIH Terrestrial System (1987)," *BIH Annual Report for 1987*, Observatoire de Paris, Paris, France, 1988.

[11] C. Boucher and Z. Altamimi, "The Initial IERS Terrestrial Reference Frame," *IERS Technical Note 1*, Observatoire de Paris, Paris, France, 1989.

[12] E. M. Standish and J. G. Williams, "Dynamical Reference Frames in the Planetary and Earth–Moon Systems," *Inertial Coordinate Systems on the Sky*, Dordrecht, Holland: Kluwer Academic Publishers, pp.173–181, 1990.

[13] O. J. Sovers, "JPL 1990-3: A 5-nrad Extragalactic Source Catalog Based on Combined Radio Interferometric Observations," *The Telecommunications and Data Acquisition Progress Report 42-106, vol. April–June 1991*, Jet Propulsion Laboratory, Pasadena, California, pp. 364–383, August 15, 1991.

[14] R. N. Treuhaft and S. T. Lowe, "A Measurement of Planetary Relativistic Deflection," *Astron. J.*, vol. 102, no. 5, pp. 1879–1889, 1991.

[15] O. J. Sovers, *Observation Model and Parameter Partials for the JPL VLBI Parameter Estimation Software MODEST—1991*, JPL Publication 83-39, Rev. 4, Jet Propulsion Laboratory, Pasadena, California, 1991.

[16] J. A. Steppe, O. J. Sovers, and S. H. Oliveau, "Smoothed Standard-Coordinate Earth Rotation From Deep Space Network VLBI," *IERS Technical Note 11: Earth Orientation, Reference Frames, and Atmospheric Excitation Functions*, submitted for the *1991 IERS Annual Report*, ed. P. Charlot, Observatoire de Paris, Paris, France, June 1992.

[17] J. G. Williams and E. M. Standish, "Dynamical Reference Frames in the Planetary and Earth–Moon Systems," *Reference Frames in Astronomy and Geophysics*, J. Kovalevsky et al., eds., Dordrecht, Holland: Kluwer Academic Publishers, pp. 67–90, 1989.

[18] C. C. Chao, *The Tropospheric Calibration Model for Mariner Mars 1971*, JPL Technical Report 32-1587, Jet Propulsion Laboratory, Pasadena, California, pp. 61–76, 1974.

[19] R. N. Treuhaft and G. E. Lanyi, "The Effect of the Dynamic Wet Troposphere on Radio Interferometric Measurements," *Radio Science*, vol. 22, pp. 251–275, 1987.

[20] H. N. Royden, D. W. Green, and G. R. Walson, "Use of Faraday-Rotation Data From Beacon Satellites to Determine Ionospheric Corrections for Interplanetary Spacecraft Navigation," *Proc. of the Beacon Satellite Symposium, COSPAR/URSI*, Warsaw, Poland, 1980.

[21] R. D. Kahn and J. S. Border, "Precise Interferometric Tracking of Spacecraft at Low Sun–Earth–Probe Angles," AIAA-88-0572, 26th Aerospace Sciences Meeting, Reno, Nevada, 1988.

[22] R. Woo and J. W. Armstrong, "Spacecraft Radio Scattering Observations of the Power Spectrum of Electron Density Fluctuations in the Solar Wind," *J. Geophys. Res.*, vol. 84, no. A12, pp. 7288–7296, 1979.

[23] J. S. Border, W. M Folkner, R. D. Kahn, and K. S. Zukor, "Precise Tracking of the Magellan and Pioneer Venus Orbiters by Same-Beam Interferometry," AAS/AIAA Spaceflight Mechanics Meeting, Houston, Texas, 1991.

[24] J. B. Minster and T. H. Jordan, "Present-Day Plate Motions," *J. Geophys. Res.*, vol. 83, pp. 5331–5354, 1978.

[25] M. H. Finger and W. M. Folkner, "A Determination of the Radio-Planetary Frame Tie and the DSN Tracking Station Locations," AIAA-90-2905, AIAA/AAS Astrodynamics Conference, Portland, Oregon, 1990.

[26] Y. Vigue, S. M Lichten, G Blewitt, M. B. Heflin, and R. P. Malla, "Precise Determination of Earth's Center of Mass Using Measurements From the Global Positioning System," *Geophysical Research Letters*, vol. 19, no. 14, pp. 1487–1490, 1992.

[27] G. Bierman, *Factorization Methods for Discrete Sequential Estimation*, vol. 128, New York: Academic Press, 1977.

[28] J. B. Thomas, *Interferometry Theory for the Block II Processor*, JPL Publication 87-29, Jet Propulsion Laboratory, Pasadena, California, October 1987.

[29] B. D. Mulhall, V. J. Ondrasik, and K. L. Thuleen, *The Ionosphere*, JPL Technical Report 32-1499, Jet Propulsion Laboratory, Pasadena, California, pp. 45–67, 1970.

Appendix A

PHOBOS Observable Processing

I. Computing Observables

In a VLBI measurement, the signal from a celestial source is recorded simultaneously by two stations. The recorded signals from the two stations are processed to obtain the signal delay between them. This interferometric delay can be written as a sum of a geometric delay plus propagation media and instrumentation effects and clock synchronization error:

$$\tau = \frac{1}{c}\vec{B} \cdot \hat{S} + \tau_{media} + \tau_{instr} + \tau_{clock}$$

where $\vec{B}$ is the baseline vector, c is the speed of light, and $\hat{S}$ is the direction to the source. Measurement of the delay is thus a measurement of the component of $\hat{S}$ along the direction of the baseline. The astrometric accuracy of a VLBI measurement depends on the ability to calibrate propagation media and instrumentation effects and synchronize clocks, and on the accuracy of the baseline and Earth orientation information used.

In a differential spacecraft–quasar VLBI measurement, the signals of a spacecraft and an angularly nearby reference quasar are recorded, and the interferometric delays for the two sources are differenced. The differenced delay can be written

$$\Delta\tau = \frac{1}{c}\vec{B} \cdot \Delta\hat{S} + \Delta\tau_{media} + \Delta\tau_{instr} + \Delta\tau_{clock}$$

where $|\Delta\hat{S}|$ is equal to the angle between the two sources. Errors in the calibration of media and instrumental effects and clock synchronization, as well as errors in the modeling of baseline and Earth orientation, largely cancel in the difference. The astrometric accuracy of this measurement of the angular separation between the two sources is thus much better than for a VLBI measurement of a single source. (In the frame-tie estimation in Section V, the delays are not explicitly differenced, but only the delay differences contribute to the frame-tie solution.) The closer together the sources, the better the common mode cancellation. Very rarely will a spacecraft be angularly close enough to an appropriate quasar for the two sources to fit into an antenna beamwidth. Therefore, typically the spacecraft and quasar are observed sequentially rather than simultaneously. The spacecraft and quasar signals are recorded alternately for intervals typically of a few minutes. Each recording interval is called a "scan."

In a VLBI measurement, the spacecraft and quasar signals are recorded at multiple frequencies at each station. Differential phase between the stations is measured at each frequency. The interferometric delay is the slope of the differential phase with frequency, so the delay precision is roughly inversely proportional to the separation of the highest and lowest frequencies.

The recorded differential phase between the two stations for a spacecraft or quasar signal of frequency ω is

$$\phi(\omega, t) = \omega\tau(t) + \phi_I(\omega)$$

where $\tau(t)$ is the interferometric delay and $\phi_I(\omega)$ is instrumentation phase, which includes an arbitrary local oscillator startup phase, filter response, and any other nonlinear phase shifts that occur in the recording system. (The instrumentation phase is generally also a function of time, but extant phase calibration

tone data indicate that instrumentation phase temporal behavior was sufficiently stable over a pass to be neglected.) The interferometric delay also has a frequency dependence due to signal propagation through the ionospheric and solar plasma which has been suppressed here for simplicity.[13] The instrumentation phase must be calibrated to get interferometric delays. Also, the cycle ambiguity of the signal phase must be resolved to get meaningful delays. The observation of the quasar enables the resolution of the spacecraft phase ambiguity.

II. Station Configuration

An example of the WCB VLBI channel configuration is shown in Fig. 8. Fourteen channels of 2-MHz bandwidth were distributed over the L-band receiver bandwidth of approximately 70 MHz. This arrangement of channels is not optimal for measuring quasar delays because these passes were originally intended as preparation for future acquisitions of VLBI data from the Phobos-2 lander. The configuration was designed to sample the bandpass of the receiver and to provide data to be used in verifying procedures for phase ambiguity resolution. Each of the 14 channels was sampled at the Nyquist rate, 4 Mbits/sec, for a total data rate of 56 Mbits/sec.

The figure also illustrates the recorded spectrum for the spacecraft. The spacecraft signal consisted of odd harmonics of a 7.4-MHz square-wave phase modulated onto the carrier. Because only the first harmonic and the -3rd harmonic provided an adequate SNR, the spanned bandwidth of the spacecraft signal was limited to 29.4 MHz. The SNR of the first harmonic was 23 dB-Hz; that of the -3rd harmonic was 12 dB-Hz.

Each spacecraft tone was typically recorded by a pair of channels offset in frequency. This provided redundancy in case of channel failure. Also, comparison of the tone phases from each channel in a pair yielded information on instrumentation phase.

It had been planned to use phase calibration tones to determine and remove instrumental errors in delay, but due to equipment failures, phase calibration tones were present at only a single station for each pass. Comparison of phase differences of single tones that appeared in a pair of channels showed no significant drift between channels.

III. Correlation

The WCB VLBI data were recorded on tape at a data rate of 56 Mbits/sec at each station. This large volume of data was processed to produce a VLBI group delay observable for each scan. The processing was done in two steps: First, the WCB tapes were correlated using model delays to compress the data to 2-sec integrations. Second, the compressed data were processed by postcorrelation software to produce group delays and ancillary data.

The WCB data were correlated using the JPL/Caltech Block II VLBI Processor [28], henceforth called "the correlator." Because the spacecraft signal consisted of discrete frequency sinusoidal "tones" and the quasar signal is broadband noise, the spacecraft and quasar scans were processed rather differently in the correlator, but the end results are similar in form.

For the spacecraft data, an a priori spacecraft trajectory was used to produce a spacecraft range model for each station, which was in turn used to produce a model for the phase of each tone at each station. The correlator correlates the recorded spacecraft signal with the phase model and integrates for 2-sec intervals. The correlator output is a time series of correlation amplitudes and residual phases

[13] B. Iijima, "Block II Processor Delta-DOR Observable Extraction," in preparation, Jet Propulsion Laboratory, Pasadena, California, 1994.

(the difference between the spacecraft phase and phase model) for each tone in each channel at each station. Differencing the correlator output phase from the two stations gives residual phase for each tone at frequency ω_i:

$$\phi_r(\omega_i, t_j) = \omega_i \tau_r(t_j) + \phi_I(\omega_i) \tag{A-1}$$

where t_j is the center of the jth 2-sec integration interval and the residual delay τ_r is the difference between the interferometric delay and the difference of the range models used to produce the phase models.

The correlator processes quasar scans by synchronizing the quasar signals in two stations' bit streams using model delays, then multiplying the two streams, correlating the resultant interferometric fringes with a differential phase model, and integrating for 2-sec intervals. This is done for each channel on each baseline. The correlator also forms a cross-power spectrum, effectively dividing each 2-MHz channel into 8 "bins" 0.25-MHz wide. The output of the correlator is a time series of 2-sec correlation amplitudes and residual phases for each bin. The residual phases for bin i can be written as

$$\phi_r(\omega_i, t_j) = \langle \omega_i \tau_r(t_j) + \phi_I(\omega_i) \rangle_{2 \text{ sec time avg}} = \omega_i \tau_r(t_j) + \phi_I(\omega_i) + \phi_{avg}(\omega_i) \tag{A-2}$$

where ω_i is the RF centroid frequency of the bin, t_j is the center time of the 2-sec integration, and the residual delay, τ_r, is the interferometric delay minus the synchronization delay model. The correlator output phase is a complicated average of the quasar signal phase over the 0.25-MHz-wide bin, and is approximately equal to the quasar signal phase at the center of the bin. The phase ϕ_{avg} represents the small discrepancy between the average phase over the bin and the phase at the center of the bin. Because of the proximity of all the sources and the relative brevity of each pass, ϕ_{avg} is approximately the same in all quasar scans during a pass.

IV. Postcorrelation Processing

The PHOBOS frame-tie experiment was the first spacecraft–quasar differential VLBI measurement using the WCB data acquisition terminals and Block II processor. New postcorrelation software[14] was developed to produce observables from the correlator output. The software compressed each scan of VLBI data to give eight numbers: a time tag and reference frequency, two VLBI observables (group delay and phase delay rate) and the system noise uncertainty on each, the instrumentation phase calibration error on the group delay, and an effective frequency for ionospheric calibration. This section briefly describes how the postcorrelation software produced these eight numbers from the array of phases in Eqs. (A-1) and (A-2).

The group delays for each scan were computed from the phases in Eqs. (A-1) and (A-2) by a three-step process: First, the time series at each frequency was compressed to a single point for each frequency. Second, the instrumentation phase was calibrated out. Third, the residual group delay was computed, and the total group delay observable was formed by restoring the delay models used in the correlator. Phase delay rates were also produced in this process. These three steps are described in some detail below.

Step 1: Phase Compression. The correlator station-differenced output residual phase can be rewritten as

$$\phi_r(\omega_i, t_j) = \Phi(\omega_i) + \omega_i f(t_j)$$

[14] Ibid.

where

$$\Phi(\omega_i) = \omega_i \tau_r(t_0) + \phi_I(\omega_i) + [\phi_{avg}(\omega_i)]$$

$$f(t_j) = \tau_r(t_j) - \tau_r(t_0)$$

The quantities $\Phi(\omega_i)$, one for each frequency, depend only on frequency, and $f(t_j)$ contains all temporal delay variations. The brackets enclosing ϕ_{avg} indicate that it is zero for spacecraft data. One can estimate Φ and f by doing a least-squares fit to the phases $\phi_r(\omega_i, t_j)$ weighted by the system noise uncertainty (which is approximately inversely proportional to the correlation amplitude). In order to make the least-squares fit well defined, it was required that a linear fit to $f(t_j)$ be zero at the scan reference time t_0. This ensured that the slope of Φ would be the group delay at the reference time. The scan reference time tag t_0, and a reference frequency ω_0 (to be used below), were computed by doing a weighted average of time and frequency over all the data for the scan.

Step 2: Instrumentation Phase Calibration. Since phase calibration tone data were not available from all stations, a technique was used to estimate the nonlinear component of the instrumental phase directly from the data. This technique is called manual phase calibration (MPC) and works as follows: A strong quasar scan is chosen to be the reference scan. The compressed phase of this reference scan is defined to be the manual phase calibration phase:

$$\Phi_{MPC}(\omega_i) = \omega_i \tau_{MPC} + \phi_I(\omega_i) + \phi_{avg}(\omega_i)$$

where τ_{MPC} is the residual delay of the reference scan.

Instrumentation phase calibration is performed on quasar scans by subtracting Φ_{MPC} from Φ to get the calibrated phase Φ_{cal}:

$$\Phi_{cal}(\omega_i) = \Phi(\omega_i) - \Phi_{MPC}(\omega_i) = \omega_i(\tau_r - \tau_{MPC})$$

To calibrate a spacecraft scan, Φ_{MPC} is interpolated to the spacecraft frequency and then subtracted from the spacecraft phase. The result is

$$\Phi_{cal}(\omega_i) = \Phi(\omega_i) - \Phi_{MPC}^{interpolated}(\omega_i) = \omega_i(\tau_r - \tau_{MPC}) + \varepsilon_{MPC}$$

where the spacecraft phase calibration error ε_{MPC} contains ϕ_{avg} interpolated to the spacecraft frequency and the discrepancy between ϕ_I and the instrumental phase interpolated between quasar bin frequencies. Because the spacecraft frequencies received at the station vary less than 1 kHz over each pass and the phase response is expected to be fairly smooth on that scale, ε_{MPC} is common to all spacecraft scans in a pass.

Analysis of a limited data set measuring the phase responses of several of the WCB video converters suggests that ε_{MPC} will be around 4 millicycles (mcyc) for most WCB video converters. However, a few of the WCB video converters deviate 10 mcyc or more from the nominal WCB nonlinear phase response, and much larger calibration errors are expected in those converters. A way of determining the size of ε_{MPC} directly from the data is discussed in Step 3.

Step 3: Computing the Group Delay Observable. A priori delay information was used to resolve the relative phase cycle ambiguity of $\Phi_{cal}(\omega_i)$ between frequencies, enabling the residual group delay,

which is the slope of Φ_{cal}, to be computed. Doing a linear least-squares fit of a line to Φ_{cal} weighted by the sum of the system noise uncertainty (including ε_{MPC} for the spacecraft) gives the measured (residual) group delay

$$\tau_r^{meas} = \tau_r(t_0) - \tau_{MPC} + [\delta_{MPC}]$$

where δ_{MPC} is the contribution of ε_{MPC} to the slope. The brackets around δ_{MPC} indicate that it is zero for quasar scans. There is a bias $-\tau_{MPC}$ in all delays. In the frame-tie parameter estimation, this will be absorbed into the clock bias parameter and have no effect on the frame-tie parameters. There is, in addition, an extra bias δ_{MPC} common to all spacecraft delays, but absent from the quasar delays, that will contribute an error to the frame tie.

An estimate of ϵ_{MPC} can be obtained by observing the scatter in the data in excess of the system noise uncertainty in the linear fit to Φ_{cal} for the spacecraft scans. An example of the residuals to the linear fit is shown in Fig. A-1. The data shown are from the March 25 pass, and the error bars displayed are system noise uncertainty. The magnitude of the instrumentation calibration error on each spacecraft channel phase was determined empirically by forcing the reduced chi-squared of the linear fit to be 1. This gave an instrumentation calibration error of about 8 mcyc in each channel phase on February 17 and 3 mcyc in each channel phase on March 25, roughly in agreement with the expected size given at the end of the discussion of Step 2.

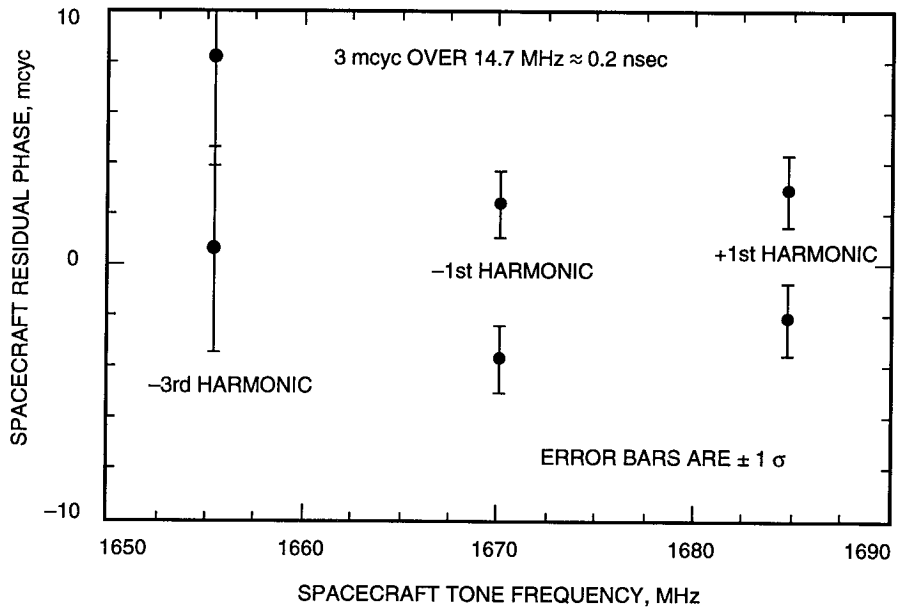

Fig. A-1. Phobos-2 instrumental phase error for Goldstone–Canberra baseline.

The system noise and δ_{MPC} both contribute to the spacecraft delay observable uncertainty, and their contributions to the uncertainty are separately computed and passed to the frame-tie estimation process. The contribution of δ_{MPC} to the delay uncertainty is a measure of the instrumental phase bias between the quasar and spacecraft scans. For the quasar scans, only the system noise uncertainty of the quasar delays is passed on to the frame-tie estimation process.

The result of the linear fit above is the residual group delay. The total group delay observable is obtained by evaluating the delay models used in correlation at the scan reference time and adding the delay model to the delay residual to get the total group delay observable.

The other observable extracted from the data, the phase delay rate, was computed by taking the slope of $f(t_j)$ from Step 1 and dividing by the reference frequency ω_0 to get the residual phase delay rate. The correlator delay rate model was then restored to get the total phase delay rate observable.

Appendix B
Faraday Calibration Error Model

Because of the relatively low frequency of the PHOBOS frame-tie observations (L-band is approximately 1.7 GHz), dispersive delays from charged particles represent a significant source of measurement error. Charged particles are encountered in the interplanetary solar plasma as well as in the Earth's ionosphere. It is the charged particle delay, differenced between the spacecraft and quasars, that corrupts the frame-tie determination. The analysis of Section IV indicates that the differential solar plasma delay should be at or below the 0.1-nsec level. Ionospheric errors are expected to be significantly larger. The total zenith daytime ionospheric delay can be 25 nsec or more at one station, with low-elevation delays approaching 100 nsec.

The general characteristics of the signal delays due to the charged particles of the ionosphere are well known. The DSN routinely monitors the ionosphere's charged-particle content along a fixed ray path by acquiring Faraday rotation data from a geosynchronous satellite at each site [20,29]. Although the calibrations from Faraday data have been applied to the PHOBOS delays, the calibrations are not perfect and the effect of these errors on the frame-tie parameter estimates must be included in assessing estimate accuracy. The use of "consider" analysis to get the sensitivity of the frame-tie solution to a scaling of the Faraday calibrations was described in Section V. However, it is also important to assess the point-to-point statistics of the ionospheric delay errors in weighting the data. Because the parameters of a linear clock model on each baseline are adjusted in the solution process, the calibration error model must specify the error statistics for differential delay after a linear drift has been removed.

A good data set that illustrates both spatial and temporal ionospheric delay variations was obtained during an experiment to detect the relativistic deflection of an electromagnetic wave by the mass of Jupiter [14]. The "planetary deflection" data consist of two VLBI passes, 3 to 4 hr in duration, from March and April of 1988. Delays were obtained for a number of quasars at a range of separation angles at both S- and X-band (2.3 and 8.4 GHz). Two sources separated by 3.7 deg were observed repeatedly. Because the ionospheric delay scales as f^{-2}, where f is signal frequency, a linear combination of the dual-frequency delays provides a measure of the station-differenced ionospheric delay. These are given in terms of nanoseconds at L-band in Fig. B-1. Note that the resulting ionospheric delay for each day contains an overall bias due to uncalibrated delay biases in the S- and X-band instrumentation. Nonetheless, temporal changes in the ionosphere during each day, as well as differences in the ionosphere between sources, are well determined from these data. Since the minimum elevation for the PHOBOS observations was 22 deg, only data above a 20-deg elevation are shown in the figure.

The major characteristics of the ionosphere observed in this data set are the increase in delay of 4–5 nsec over the pass and the offset of about 2 nsec between sources. The delays show a fairly linear variation. For the analysis of the PHOBOS VLBI data, a linear clock model is removed; as a result, any linear variation common to the spacecraft and quasar will be absorbed by the clock solution. The remaining point-to-point scatter, which is due to small-scale ionospheric irregularities, will manifest itself as an additional noise source for the observed delays. In addition, any bias between the spacecraft and quasar ionospheric delays will directly corrupt the frame-tie estimate.

In Fig. B-2, the same planetary deflection data are shown after Faraday calibrations have been applied. The calibrations have reduced the delay drift over each pass by a factor of 2, but drifts of 0.6–1.5 nsec per hour remain. The bias in differential delay between sources has decreased, to 0.2 nsec for the first pass and 0.7 nsec for the second. The latter bias roughly corresponds to an error in relative position of 30 nrad.

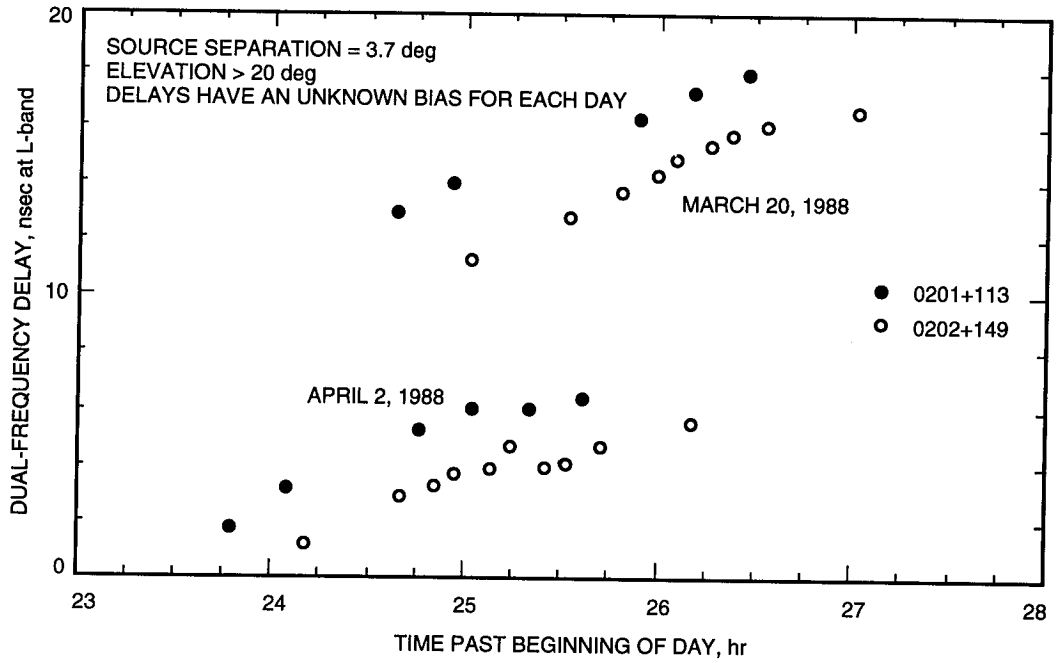

Fig. B-1. Ionosphere delay from dual-frequency VLBI.

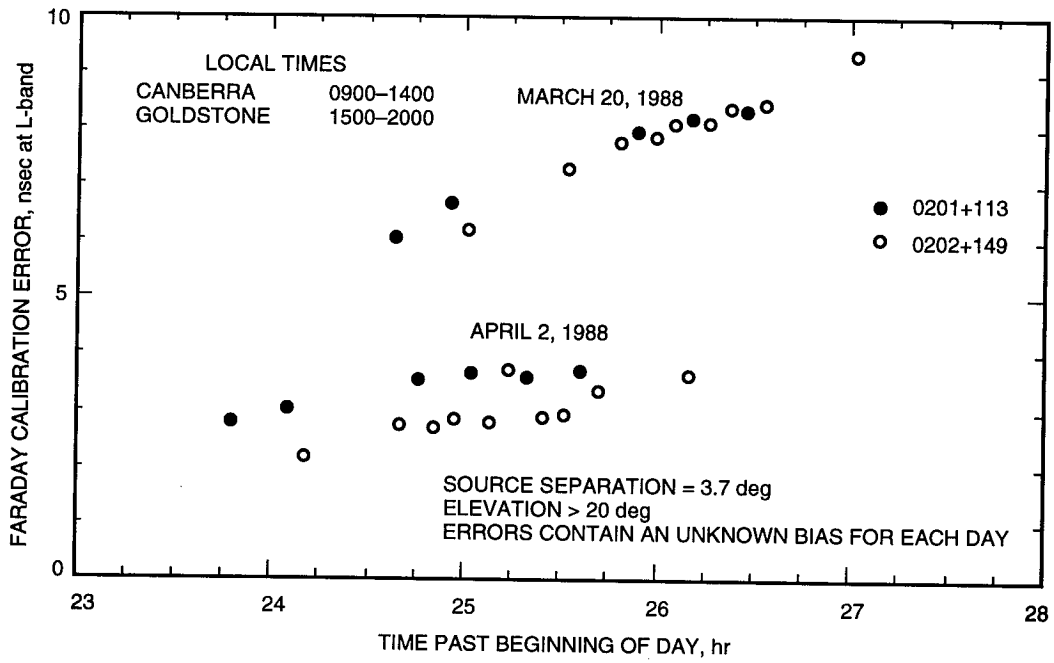

Fig. B-2. Error in Faraday calibration of ionosphere delay.

Given that nanosecond-level differential ionospheric delay biases can remain after Faraday calibration for angular separations of 3–4 deg, it is reasonable to include delays only for the quasar closest to the Phobos-2 spacecraft on each day in the nominal frame-tie solution. This corresponds to spacecraft-quasar angular separations of 1.0 deg for the February 17 pass and 0.4 deg for the March 25 pass. The angular separations from the Phobos-2 spacecraft of other quasars observed in these two experiments ranged from 3.2–5.6 deg, and hence were expected to have significantly larger ionospheric delay biases relative to the spacecraft scans.

Another benefit of using only the closest quasar is that it simplifies the modeling of the point-to-point error statistics. The spatial separation at the peak ionospheric altitude of 350 km for a pair of ray paths separated by 1 deg will be much smaller than the temporal displacement of the ray path due to Earth rotation during the 5-min time interval between adjacent scans. Thus, to a good approximation, we can represent the point-to-point scatter of the spacecraft and primary quasar scans based on statistics derived for ionospheric fluctuations along a single line of sight.

To quantify these fluctuation statistics, several days of dual-frequency (S-/X-band) observations of the Magellan spacecraft in orbit about Venus have been examined. The data were collected simultaneously at California and Australia during February 1991. Phase observations of the S-band and X-band carrier signals were made continuously at 2-sec intervals for a period of several hours. The spacecraft elevations ranged from 20–50 deg at the two stations. The passes occurred at midafternoon in California and midmorning in Australia.

Dual-frequency phases from each station were linearly combined to track variations in electron (el) density integrated along the line of sight (TEC_{los}) according to

$$\phi_S(t) - \frac{3}{11}\phi_X(t) = -0.54 \times TEC_{los}(t) + bias + solar\ plasma$$

where phase is in cycles and TEC_{los} is in units of 10^{16} el/m^2 (one TEC is about a 0.5-nsec delay at L-band). The single-station data show significant solar plasma fluctuations. Differencing this quantity between the California and Australia stations greatly reduced the solar plasma error, leaving a precise measure of variations in the station-differenced line-of-sight electron density ΔTEC_{los}. Figure B-3 shows an example of the variability of ΔTEC_{los} over about a 1-hr time span, after removal of a straight line. The ΔTEC_{los} is observed to vary by about $\pm 1 \times 10^{16}$ el/m^2 over the 1-hr span. From these data, the structure function (the expected mean-square change in ΔTEC_{los} over an interval T) was calculated as

$$D_{TEC}(T) \equiv \left\langle [\Delta TEC_{los}(t+T) - \Delta TEC_{los}(t)]^2 \right\rangle$$

Figure B-4 depicts four structure functions derived from Magellan S-/X-band data collected on two different days of the year (DOY). All the structure functions exhibit power-law slopes close to 1, characteristic of a random walk process. The straight line in the figure is the result of a fit of the four structure functions to a random walk model of the form $D_{TEC}(T) = C^2T$. The random walk amplitude C is found to be

$$C = 1.80 \times 10^{14} \frac{\text{el}}{\text{m}^2\sqrt{\text{sec}}}$$

Converting to the delay variation at the 1.7-GHz PHOBOS frequency yields $C = 8.3 \times 10^{-3}$ nsec/$\sqrt{\text{sec}}$, or about a 0.26-nsec variation in 1000 sec. Although the examined data set is limited, it nonetheless serves

to guide the choice of random walk process noise and sets the a priori value of the random walk amplitude. The actual amplitude was adjusted in the course of parameter estimation to yield a satisfactory value of χ^2. For the reference solution, the adjusted amplitude was equivalent to a 1-σ error of 0.5 nsec in 1000 sec.

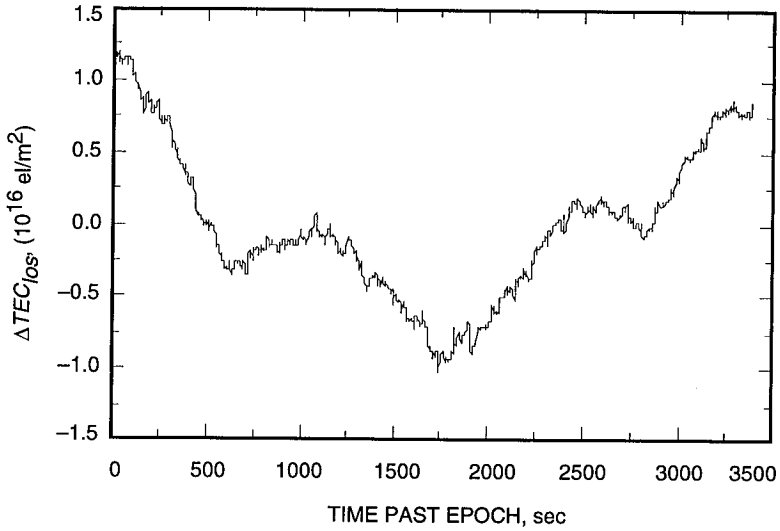

Fig. B-3. Line-of-sight station-differenced integrated electron content variations derived from S-/X-band carrier phase observations of the Magellan spacecraft after removal of a linear fit (DOY 048, 1991, Goldstone–Canberra).

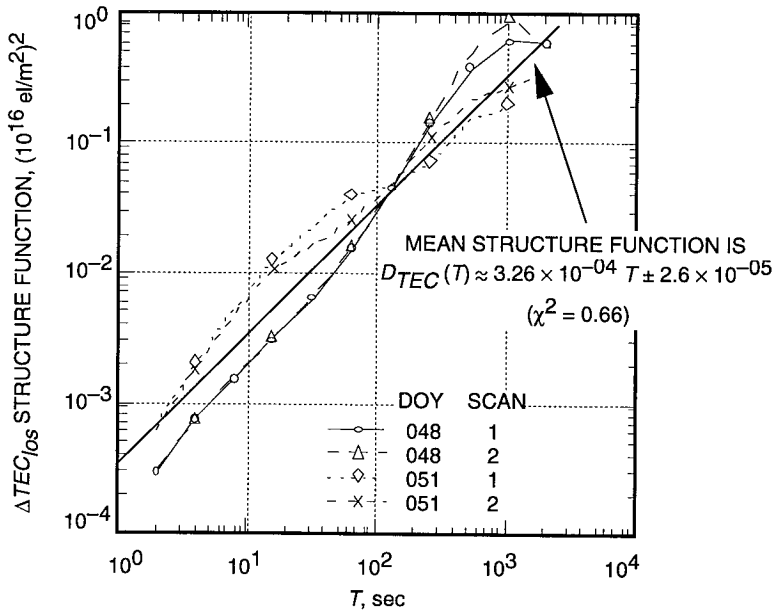

Fig. B-4. The ΔTEC_{los} structure functions derived from dual-frequency observations of the Magellan spacecraft (Goldstone–Canberra, 1991). A fit of the four structure functions to a random walk model yields a random walk amplitude C of 1.8 x 10^{14} el/m^2/$\sqrt{\text{sec}}$ (= 0.26 nsec at 1000 sec at L-band).

In summary, the nominal PHOBOS frame-tie result was based on quasar delays only for the sources closest to the Phobos-2 spacecraft on each day because of significant uncertainty in the statistical characterization of postcalibration ionospheric delay errors for angular separations of a few degrees or more. Examination of several time series of station-differenced dual-frequency spacecraft data yielded a random walk model for the point-to-point ionospheric delay fluctuations, which was used in the final frame-tie estimation. The sensitivity of the frame-tie solution to an overall scaling error in the Faraday calibrations was also determined. Several alternative solutions were also computed, including two using all of the observed quasars (one with random walk ionosphere noise and one without). The differences from the reference solution are all within the stated accuracy. In no case was the ionosphere the dominant error in the final frame-tie estimate.